

# Measurement and Validation of Magnetic Lenses

for Electron Beam Melting

Master's thesis in Wireless, Photonics and Space Engineering

CALLE MALM



MASTER'S THESIS 2018:10

# Measurement and Validation of Magnetic Lenses

for Electron Beam Melting

CALLE MALM



**CHALMERS**  
UNIVERSITY OF TECHNOLOGY

Department of Space, Earth and Environment  
*Division of Astronomy and Plasma Physics*  
CHALMERS UNIVERSITY OF TECHNOLOGY  
Gothenburg, Sweden 2018

Measurement and Validation of Magnetic Lenses  
for Electron Beam Melting  
CALLE MALM

© CALLE MALM, 2018.

Supervisor: David Svensson, Arcam EBM  
Examiner: Hans Nordman, Department of Space, Earth and Environment

Master's Thesis 2018:10  
Department of Space, Earth and Environment  
Division of Astronomy and Plasma Physics  
Chalmers University of Technology  
SE-412 96 Gothenburg  
Telephone +46 31 772 1000

Cover: Visualisation of magnetic field perpendicular to optical axis mapped in three planes inside an astigmatism lens.

Typeset in L<sup>A</sup>T<sub>E</sub>X  
Gothenburg, Sweden 2018

Measurement and Validation of Magnetic Lenses  
for Electron Beam Melting  
CALLE MALM  
Department of Space, Earth and Environment  
Chalmers University of Technology

## Abstract

Magnetic lenses are crucial components in the electron beam melting process used for 3d-printing at Arcam. Validating that the lenses going into machine production are within specification is important. Therefore, this thesis has modified and confirmed a measurement setup, the field mapper, to be used for measurement and validation of magnetic lenses. The field mapper was then used to investigate normal behaviour of the focus and deflection lenses going into machine production as well as recreating defects of faulty lenses of the deflection and astigmatism lens to ascertain if machine integrity is compromised for respective defect. The focus lens revealed a non-significant spread, the deflection lens presented a wider spread that is easily compensated for in the machine calibration process, and for the comparison between an astigmatism lens to the same lens with an introduced winding error a significant change in the centre of zero-field was seen.

Keywords: Magnetic lens, electron beam melting, electron optics, focus, deflection, astigmatism.



## Acknowledgements

I would like to thank all the people at Arcam that has helped with various issues, alteration of equipment and engaging discussions of my problems. Big or small there has always been someone that has taken me under their wings and helped out. This especially encompasses the beam team who has both welcomed me as part of their team and helped me achieve what is presented in this thesis. A special thanks goes out to David Svensson, my supervisor at Arcam, also part of beam team, for guidance forward as well as being my pillar of knowledge and understanding throughout the project. Another person critical for the completion of the thesis is my examiner Hans Nordman that has believed in me and supported me all through the thesis.

Calle Malm, Gothenburg, October 2018



# Contents

<b>List of Figures</b>	<b>xi</b>
<b>List of Tables</b>	<b>xiii</b>
<b>1 Introduction</b>	<b>1</b>
1.1 Background . . . . .	1
1.2 Aim . . . . .	1
1.3 Demarcations . . . . .	2
1.4 Ethical, Societal and Sustainability Aspects . . . . .	2
<b>2 Theory</b>	<b>5</b>
2.1 Brief History of Electron Optics . . . . .	5
2.2 Lorentz Force . . . . .	5
2.3 Magnetic Lenses . . . . .	6
2.3.1 Solenoid . . . . .	6
2.3.2 Dipole Lens . . . . .	7
2.3.3 Quadrupole Lens . . . . .	8
2.4 Focus Coil Simulations . . . . .	9
<b>3 Methods</b>	<b>11</b>
3.1 Initial Measurement Rig . . . . .	11
3.1.1 LabVIEW . . . . .	11
3.1.2 Coordinate System in the Measurement Rig . . . . .	13
3.2 Measurement Outline . . . . .	13
3.2.1 Repeatability Measurements . . . . .	13
3.2.2 Resolving Average Coil Behaviour . . . . .	15
3.2.3 Coil Winding Errors . . . . .	15
3.3 Data Processing . . . . .	15
3.4 MATLAB code . . . . .	16
<b>4 Results</b>	<b>17</b>
4.1 Measurement Repeatability . . . . .	17
4.1.1 Probe to Coil Alignment . . . . .	17
4.1.2 Field Probe . . . . .	18
4.1.3 Trigger Data Acquisition . . . . .	19
4.1.4 Measurement Point Density . . . . .	22
4.1.5 Instrument Parameters . . . . .	23

4.1.5.1	Frequency Generator . . . . .	23
4.1.5.2	Oscilloscope . . . . .	24
4.1.6	Final Measurement Rig . . . . .	26
4.2	Probe Calibration . . . . .	27
4.3	Average Lens Measured Data . . . . .	28
4.3.1	Focus Lens . . . . .	29
4.3.2	Deflection Lens . . . . .	31
4.4	Coil Winding Errors . . . . .	32
4.4.1	Deflection Lens . . . . .	33
4.4.2	Astigmatism Lens . . . . .	33
<b>5</b>	<b>Discussion</b>	<b>37</b>
5.1	Measurement Uncertainties . . . . .	37
5.2	Trigger Data Acquisition . . . . .	38
5.3	Average Correct Coils . . . . .	38
5.4	Coil Windings Errors . . . . .	39
5.5	Future Work . . . . .	39
<b>6</b>	<b>Conclusion</b>	<b>41</b>
	<b>Bibliography</b>	<b>43</b>

# List of Figures

2.1	Cross section along the optical axis of a focus lens with force exerted on the electron shown. The rotation caused by the focus Lens is not shown. . . . .	7
2.2	A dipole seen perpendicular to the optical axis shows a static deflection field going from pole to pole. . . . .	7
2.3	Deflection lens seen perpendicular to the optical axis is depicted showing the possibilities of rotating the deflection field inside the lens. . .	8
2.4	Quadrupole lens seen perpendicular to the optical axis with field lines running between the poles. . . . .	9
2.5	Centre plane of a half focus coil with resulting field lines are shown to the left and to the right is the magnitude of the field along the optical axis. . . . .	9
3.1	Picture of the initial measurement rig with most of the rig assembled missing only one amplifier rack. . . . .	12
3.2	An overview of the LabVIEW graphical user interface. . . . .	13
3.3	Coordinate system used in field mapper and in the thesis. . . . .	14
4.1	Added aluminium base plate with V-shaped holders and stepper motor assembly lined up. New carbon fibre probe is also visible. . . . .	18
4.2	Focus lens measurements using the current probe as trigger signal on the top and using the frequency generator as trigger signal in the bottom. Optical axis into the coils in mm at X-axis and average plane field magnitude in arbitrary units on Y-axis. . . . .	20
4.3	Difference between two different peaks from the same amplifier for the same input signal is show with red lines. The blue lines represent the signal going into the amplifier from the frequency generator. The magenta lines represent the signal out from the amplifiers into the coil. . . . .	21
4.4	Difference between amplifier out for deflection X amplifier on the left against deflection Y amplifier out on right. Blue lines represents reference signal from frequency generator signal and magenta lines represent signal going out from amplifier into the coil. . . . .	21
4.5	Comparison of using frequency generator and using the current feedback measurement from the amplifier as trigger signal over different frequencies. . . . .	22
4.6	The different point spreads as seen in LabVIEW with 37 points on the left and 225 points on the right. . . . .	22

4.7	Showing of resolution difference using 37 points per plane in the left images versus 225 points per plane in the right for the astigmatism coil.	23
4.8	Frequency dependence of the output of the amplifiers (green) compared to frequency generator output at 3kHz in the top picture and 20kHz in the bottom picture . . . . .	24
4.9	Magnitude in graphs is consistently frequency dependent for four different measurement criteria. . . . .	25
4.10	Figure showing magnitude consistency for plotting plane average, only centre point, max difference in plane and standard deviation over frequencies 1kHz and 3 kHz over the two sampling rates 1MS/s and 10MS/s. . . . .	25
4.11	Difference between not using low pass filter on the field signal in the top graph compared to using 20MHz low pass filter on the field signal in the bottom graph. Especially visible looking at the yellow signal. . . . .	26
4.12	Depicting the setup of the final measurement rig. . . . .	27
4.13	The least square fit line fitted to the average focus coil data is shown in the top graph and the residual of the fitting is displayed in the lower graph. . . . .	28
4.14	Centre point measurement of X-field for five different focus lenses. . . . .	30
4.15	Full interior point spread measurement of five different focus lenses with the average of the data of X-fields in left graph and YZ-Field in the right. . . . .	30
4.16	Full interior point spread measurement of five different focus lenses split into outer, mid and inner circle areas with respective average X-fields. . . . .	31
4.17	Full interior point spread measurement of five different focus lenses split into outer, mid and inner circle areas with respective average YZ-fields. . . . .	31
4.18	Full interior point spread measurement of five different deflection lenses split into outer, mid and inner circle areas with respective average YZ-fields. . . . .	32
4.19	Full interior point spread measurement of an unaltered deflection lens and for two alterations removing varying lengths of wire from the same lens split into outer, mid and inner circle areas with respective average YZ-fields. . . . .	33
4.20	Full interior point spread measurement of an unaltered deflection lens and for two alterations removing varying lengths of wire from the same lens split into outer, mid and inner circle areas with respective average YZ-fields. . . . .	34
4.21	Mid section of the astigmatism was measured and then some turns was dewound and removed, the two measurements are compared above.	35

# List of Tables

3.1	Measurement equipment used in the initial setup. . . . .	12
4.1	Measurement equipment used in the final setup. . . . .	26
4.2	Parameters used in the measurements . . . . .	29
4.3	Point spread for the two focus lens measurements . . . . .	29
4.4	Specific focus lens parameters . . . . .	29
4.5	Point spread for the three deflection lens measurements . . . . .	32
4.6	Specific deflection lens parameters . . . . .	32
4.7	Point spread for the astigmatism coil measurements . . . . .	34
4.8	Specific astigmatism coil parameters . . . . .	34



# 1

## Introduction

### 1.1 Background

Arcam is a company working with electron beam melting, EBM, in 3d-printers for additive manufacturing with metals. The electron beam is controlled and shaped through the use of magnetic lenses made up of magnetic coils to melt metal powder in layers to create 3d-structures. Beam size and shape is highly affected by the winding pattern of the coils. Thus, making the products very sensitive to errors in these lenses. Today there is a theoretical understanding of the ideal lenses. However, actual measurement data and categorisation of the errors and to what extent they affect the product is unknown.

### 1.2 Aim

The purpose of this thesis work is to validate the measurement setup and to understand how the magnetic lenses behave compared to the theory. To find faults and categorise these magnetic lenses. The work will, after validating the measurement setup, focus on validating measurements of the coils and assertion if reality is consistent with the theoretical ideal, with comparisons to already existing simulation results.

A measurement setup capable of validation and categorisation of the magnetic lenses is the end-product along with a start of the categorisation. This will be developed to be able to assess and validate the magnetic lenses going into production. A well-made categorisation could possibly enable error correction or yield understanding of lenses both in software and on actual coil. If correction is not possible it gives guidelines to see if the lens could be improved or what lenses need to be discarded. A majority of the work will be regarding the measurement rig and to familiarise with the settings, possibilities and constraints. To modify the hardware and software of the rig to assure that measurements can be done in a repeatable way. Thus, eliminating systematic errors and address random errors in the measurements.

After setting up the measurement rig the second objective will be to measure a set of coils each for the astigmator lens, focus lens and deflection lens. This will be done on what is believed to be correctly wound coils to assert normal behaviour of each coil type.

When normal behaviour of these lenses has been determined, the next step is to see what the effect on the lenses are if one of the windings is missing or out of place. Tests will be performed where the windings will be redistributed incorrectly to see if the error is significant or negligible. Various asymmetries and winding impairments will be tested.

The different errors for the different lenses will be categorised with the ambition to allow extended quality control of incoming lenses from manufacturer in production.

### 1.3 Demarcations

Designing new coils or suggest changes to existing coils will not be done due to time constraints and complexity. The work will be focused on the existing coils and the current possible errors.

Extensive analysis into the various parts of the measurement system will not be done. Limited investigation into different topics will be done such as effects from frequency dependence and sampling rate but a deeper analysis is excluded due to time constraints.

This thesis work will exclude the electron beam itself, especially the generation of the beam. The transfer of the beam through the lenses will be touched upon but focus will lie on the lenses and lens field components and errors they might present.

Effects from the build environment excluding electromagnetic interference, possible temperature dependence and vacuum pressure, will not be considered. This is excluded to be able to narrow down the subject as well to keep it relevant.

Simulation and an extensive theoretical investigation will also be excluded since that work has already been done at the company. Focus will instead be on the measurements to validate their work.

### 1.4 Ethical, Societal and Sustainability Aspects

Using 3D-printing or additive manufacturing instead of ordinary production methods can drastically reduce the material and energy needed. Cumulatively between

93-217 million tons of CO<sub>2</sub> emissions could be avoided by 2050 as well as thousands of tons of aluminium, titanium and nickel alloys every year in the aircraft industry alone [1]. 3d-printing is a disruptive technology that can ease production of a wide variety of complex structures. The variety of shapes and sizes that can be made enables the technology to act as an on-demand component producer situated close to the end consumer. This can reduce the need of keeping a wide stock of products or spare parts as well as reducing the shipping of products which both has environmental and societal benefits [2]. A big difference compared to cast titanium is that the additive manufacturing only requires minor surface processing, whereas with the cast titanium you get a block of metal through the kroll process to be processed to get the shape needed [3]. Thus, saving time, energy and requiring less tools.

The titanium used in Arcam's EBM machine is recyclable and very little material is wasted in the builds since most excess titanium powder is reclaimed and can be used again in the machine after sifting [4].



# 2

## Theory

Electron optics is used to describe the motion of an electron through electromagnetic fields, the synergy between electrons within a beam and beam diffraction and interaction with a specimen. It is an area of physics that use accelerated electrons that are guided through magnetic lenses. Depending on what kind of lens is used the electron beam can be focused and aberrations of the beam shape can be mended. The beam can in the same manner be deflected by a magnetic lens. The use of the wording electron optics and lenses is due to the similarities in the way you can describe electron optics compared to regular light optics. Electron optics is part of the field charged particle physics.

### 2.1 Brief History of Electron Optics

Electron optics was first introduced in 1927 when Hanz Busch ascribed the effect an axially symmetric coil had on electrons and the coil's focal length [5], introducing the electron optics nomenclature. This was followed by Max Knoll and Ernest Ruska that in the early 1930's combined different coils into what would become the world's first electron microscope [6]. Despite the poor resolution achieved by the microscope Ernest Ruska and Max Knoll theoreticized the resolution limit to be  $2.2\text{\AA}$  which was reached 40 years later [6]. The research around electron optics has since then evolved into a myriad of uses: such as scanning and transmission electron microscopes, electron etching and for the subject of this thesis electron beam melting.

### 2.2 Lorentz Force

The force that explains how the motion of the electron changes through the magnetic fields is called the Lorentz Force [7]. The Lorentz Force also dictates how the electric field affect the charged particle, which for the use in this thesis is disregarded and the electric field component is assumed to be zero. The simplified formula giving

the magnetic force is written as

$$F_m = q \cdot v \times B \quad (2.1)$$

where  $q$  is the elemental charge,  $v$  is the velocity vector in meter per second [m/s] of the electron and  $B$  is the magnetic flux in Teslas [T]. This equation shows us how the magnetic force exerted on the electrons is directed at a right angle to the velocity of the particle and the magnetic field. Given the fact that the Lorentz force is dependent on the velocity of the electron the beam will showcase a chromatic dispersion. A greater force will affect the higher velocity electrons resulting in an often-unwanted spread of the beam. A variation of the velocity in the beam could be due to ripple in the accelerating electric field.

### 2.3 Magnetic Lenses

The Lorentz Force from equation 2.1 is vital to the design of the magnetic coils used in Arcam EBM machines. Following this will be a short introduction to the different coils used, their layout and functionality.

#### 2.3.1 Solenoid

The solenoid consists of a single wire wound around a bobbin encompassing the optical axis. Current flows in one direction in the wire, resulting in a magnetic field within the coil aligned along the optical axis. The fringe fields of the coil will be angled away from the optical axis back towards the coil. The magnetic field exerts a force on the electrons not travelling parallel to the optical axis causing a rotation and a condensing or focusing effect on the electron beam [8]. This is depicted in figure 2.1.

The focus coil or focus lens is a solenoid used to focus the electron beam. Consisting of a single wire wound in layers around a cylindrical bobbin, the focus lens geometry is very simple. However, the simple coil geometry does not protect against slight manufacturing errors introducing asymmetries in the lens. These asymmetries will affect the electrons with varying focusing power depending on the distance from the optical axis introducing axial astigmatism [8].

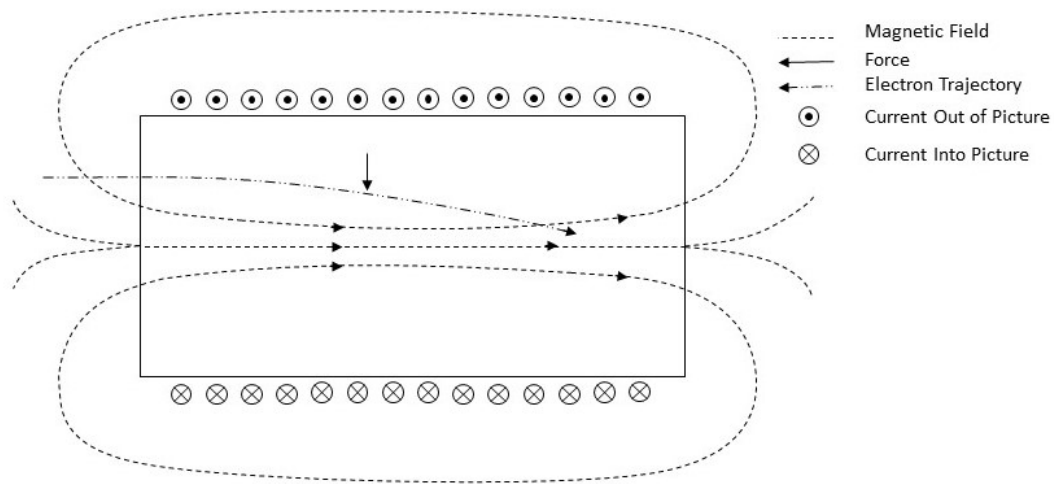


**Figure 2.1:** Cross section along the optical axis of a focus lens with force exerted on the electron shown. The rotation caused by the focus Lens is not shown.

### 2.3.2 Dipole Lens

A dipole lens is built by placing a pair of poles, oriented in the same direction, parallel to the optical axis. The resulting field is perpendicular to the optical axis. Thus propagation is from one half of the cylindrical coil to the other half as is shown in figure 2.2.

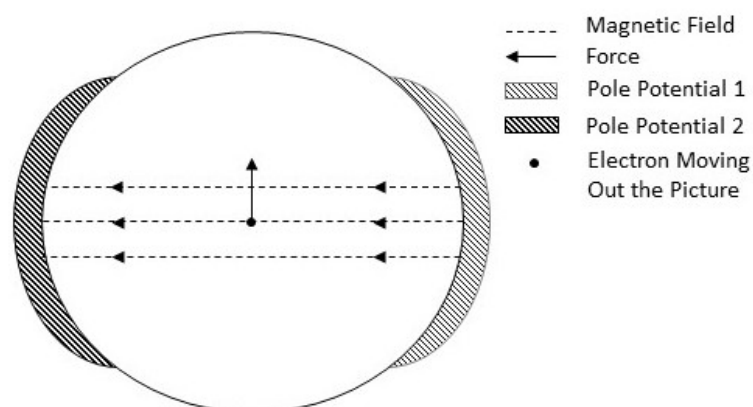


**Figure 2.2:** A dipole seen perpendicular to the optical axis shows a static deflection field going from pole to pole.

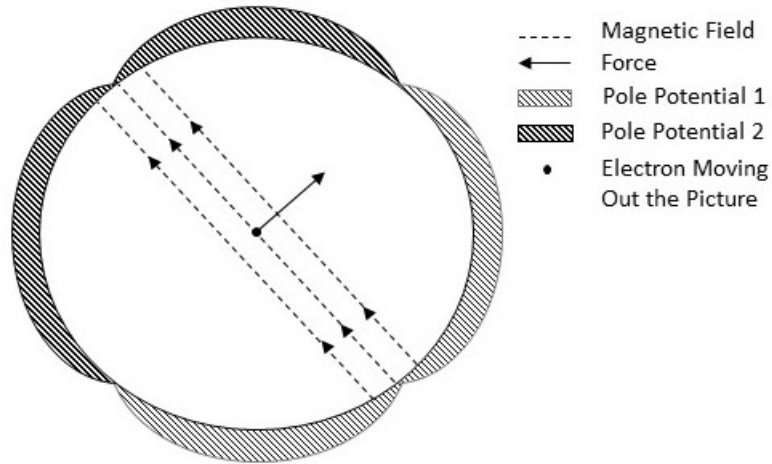


**Figure 2.3:** Deflection lens seen perpendicular to the optical axis is depicted showing the possibilities of rotating the deflection field inside the lens.

The deflection coil measured on in this thesis is comprised of two dipole pairs that are shifted 90 degrees to each other, resulting in a 90-degree shift between the individual poles. The current flowing through the two pairs is adjusted in magnitude and polarity to enable turning the field inside the coil 360 degrees allowing deflection of the beam in all direction according to the Lorentz Force as depicted in figure 2.3.

### 2.3.3 Quadrupole Lens

The quadrupole consists of two poles geometrically spaced 180 degree to each other with two poles of opposite polarisation shifted 90 degrees as depicted in figure 2.4. This results in an ideal zero-field at the centre of the coil [9].

Consisting of two quadrupoles rotated 45 degrees apart, the astigmatism coil is used to compensate for the ovalities in the beam shape introduced by differences in vertical and horizontal foci. These differences are introduced from different sources in the system. Asymmetries in the beam generation can introduce angle variations from the optical axis. Alignment issues in the mechanical assembly of the system also affects the stigmatism of the beam. As described above the focusing lens is also a source of astigmatism.

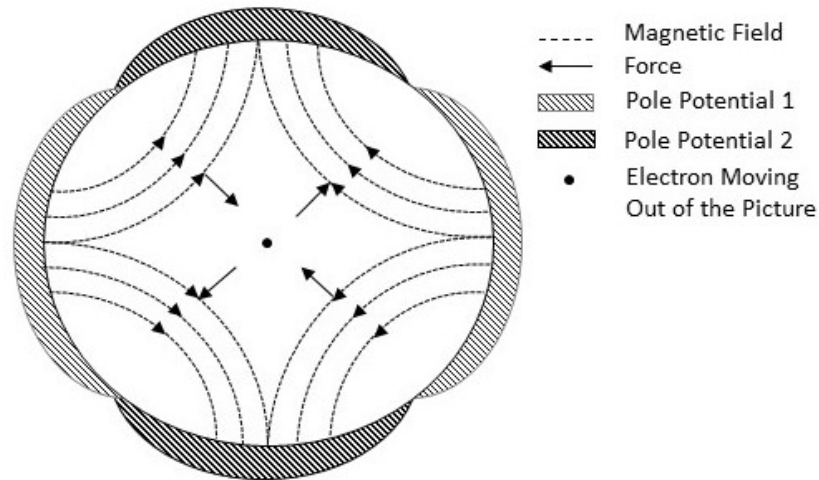


**Figure 2.4:** Quadrupole lens seen perpendicular to the optical axis with field lines running between the poles.

## 2.4 Focus Coil Simulations

Prior simulations of the focus coil, simulated at Arcam by Ali Safdar, will be introduced in order to give a rough estimate of values that is expected to be measured. Focus coil field lines from simulations is shown in figure 2.5. The figure also depicts the magnitude along the optical axis of the coil. The coil is wound with 360 turns and 3 amperes is run through the wire. The simulations were done in COMSOL Multiphysics.

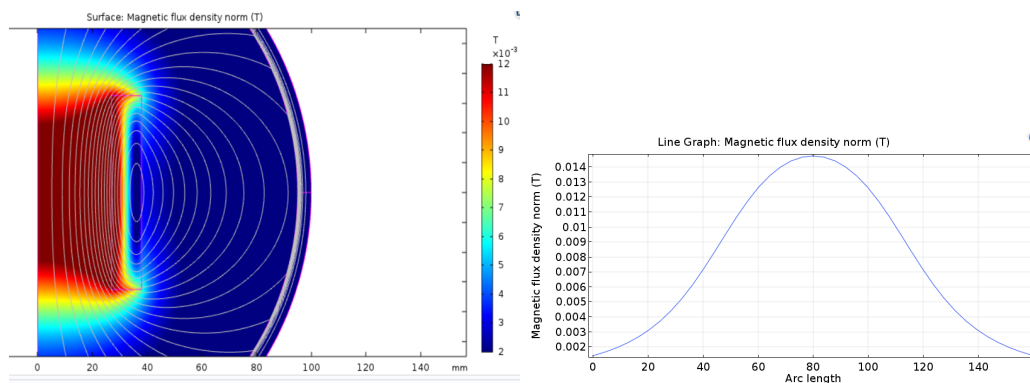


**Figure 2.5:** Centre plane of a half focus coil with resulting field lines are shown to the left and to the right is the magnitude of the field along the optical axis.



# 3

## Methods

Described in the following sections is the starting measurement rig provided by Arcam and the individual parts and their functionality. In this chapter the measurement setup and what measurements will be presented as well as the background to them will be defined. An overview of the data processing routine will also be presented.

### 3.1 Initial Measurement Rig

An early picture of the initial measurement rig is shown in figure 3.1 showing most of the equipment. The rig consists of an acrylic base plate with three stepper motor positioning stages. A separate plastic cube with a v-shaped cut out is used as coil mount. The longer X-axis stage is mounted on the base plate. The Y- and Z-stage is mounted on top of the X-stage to achieve the three-dimensional movement. Steering is done by sending commands from the LabVIEW program on the laptop to the control box. When the measurement probe reaches the LabVIEW dictated position, the control box sends out a trigger to the oscilloscope to sample the fields picked up with an X-axis coil and interchangeable Y-, Z-axis coil in top of the measurement probe. The oscilloscope also samples the current using a current probe that measures the incoming current to the coils from the amplifier outputs. A frequency generator that provides steering signal to the amplifiers dictates form, frequency and amplitude of the changing magnetic field. The power supply is used as output enabling signal to the amplifiers instead of the normal control signals usually available in the machines. All of the measurement equipment used in the initial setup is listed in table 3.1.

#### 3.1.1 LabVIEW

The LabVIEW program introduced in section 3.1 has a graphical user interface that is used to see current position of the field probe in the measurement series and

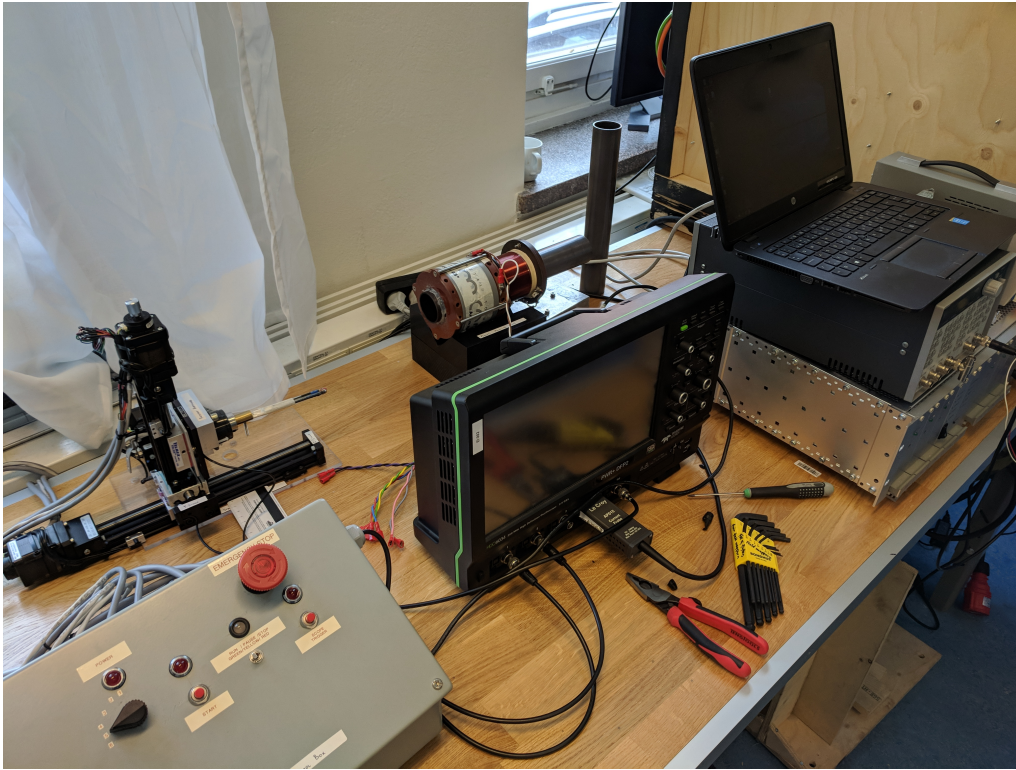


**Figure 3.1:** Picture of the initial measurement rig with most of the rig assembled missing only one amplifier rack.

**Table 3.1:** Measurement equipment used in the initial setup.

Equipment	Model	Serial no	Internal No
Oscilloscope 1 Lecroy	HDO6034	LCRY3556N06023	El 003
Current probe	AP015	A1876	El 018
Frequency Generator	BK Precision 4052	388G17108	N/A
Focus Amplifier Rack	Arcam 103819-05	17450009	N/A
Ast/ Deflection Amplifier Rack	Arcam 103818-04	17450007	N/A
Power Supply	Peak Tech 6135	0415363004532	El 027
Field Probe	Glass probe	N/A	N/A
Field Mapper Control Box	N/A	N/A	N/A
Stepper motors	N/A	N/A	N/A

generate the measurement positions within the specified dimensions as can be seen in the top of figure 3.2. The figure also depicts error messages, file handling and current status. The key features are the measurement point generation system as well as the overall measurement control. The control the LabVIEW program has on the rest of the system is as follows; it dictates and supplies the stepper motor control box with the selected position, records achieved position and sends out the signal to the control box to send the trigger signal to the oscilloscope.

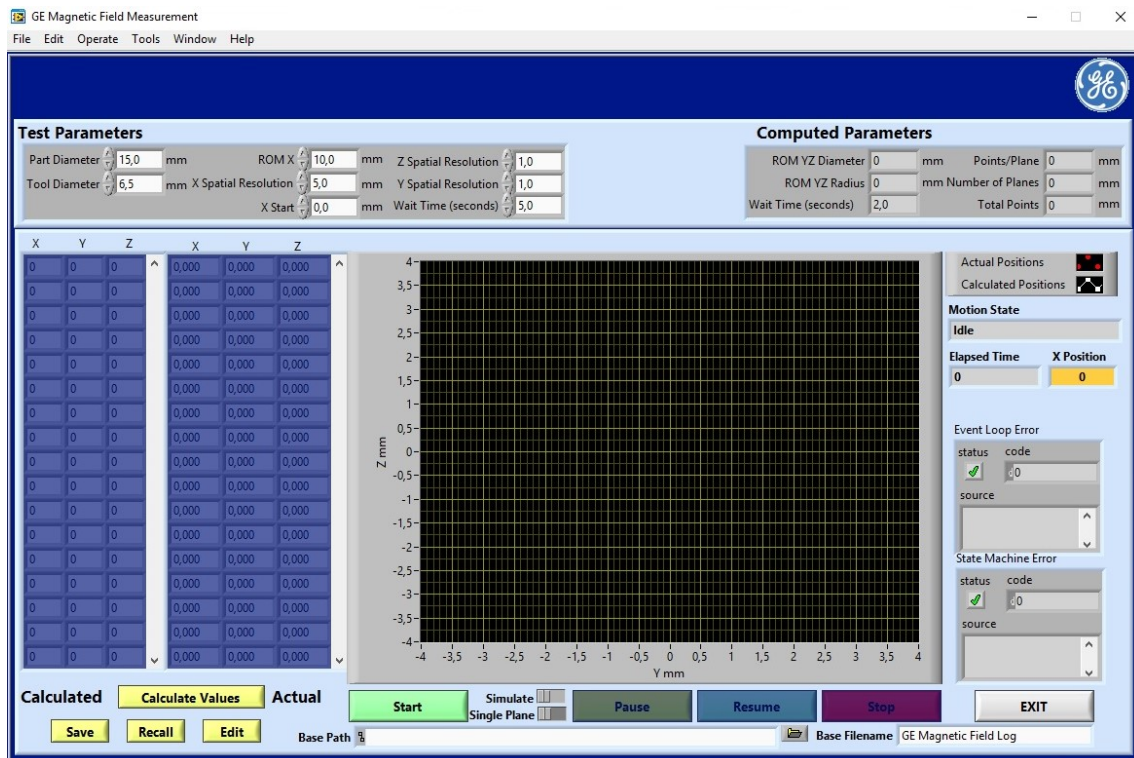


Figure 3.2: An overview of the LabVIEW graphical user interface.

### 3.1.2 Coordinate System in the Measurement Rig

X-axis in the rig refers to the optical axis going into the coils, whereas the Y and Z axis are the horizontal and vertical axis respectively. This is illustrated in figure 3.3

## 3.2 Measurement Outline

In this section the general methodology used when conducting the measurements will be described. The measurements were split into three main areas: to validate repeatability of the measurement process, to measure a set of correct coils to see variation in accepted coils and finally, miss-wound coils to see how an error of a miss-wound coil presents itself.

### 3.2.1 Repeatability Measurements

Initial testing will be focused on achieving repeatable measurements. To achieve a repeatable measurement, defined as repeatable when the measurement does not differ significantly, many measurements will take place to determine all the factors

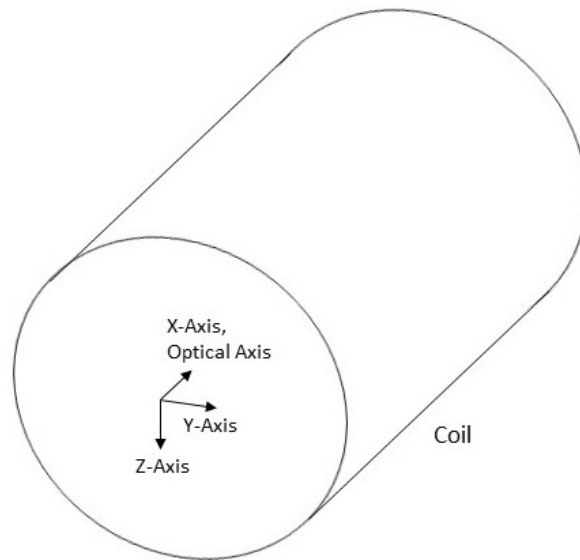


**Figure 3.3:** Coordinate system used in field mapper and in the thesis.

that introduces uncertainties. Changing one parameter, piece of equipment or way of measurement at a time. This is done to systematically determine the individual sources of ambiguity in the system.

All three coils will be used in assuring repeatable measurements however the focus coil will be primarily used. The reasoning being that the focus coil is not shielded, and the field produced by a solenoid is the most predictable out of the three since it is rotationally symmetric. The testing will be carried out on a single coil to ensure that no potential variance of the coils clouds the results. After focus coil measurements the deflection and astigmatism coil will be used to ensure that measurements on also those coils are repeatable.

Uncertainties can be introduced by a myriad of different faults. Repeatable measurements of magnetic fields are not trivial. The use of coils to pick up the field also pick up fields by nearby sources as well as noise. Noise is also introduced in the cables between the measurement equipment. A consistent alignment and positioning of both instruments and specimen is also crucial.

Getting high accuracy measurements also introduces more factors to experiment with. Among those are oscilloscope sampling rate, sampling window and frequency. Frequency to make sure no significant resonance is present and to check the frequency dependence of field probe and amplifiers. Sampling rate to determine that no information is lost. Sampling window to be large enough to reliably get big enough measurement samples.

### 3.2.2 Resolving Average Coil Behaviour

These measurements will be focused on establishing a data set of assumed correct coils. This data set will be used as a base to determine average coil behaviour and variance. Testing will be on a set number of coils for two of the different coil types, focus and deflection. Numerical values will thereafter be processed and compared in disparate ways according to coil type.

### 3.2.3 Coil Winding Errors

In this series measurements will be focused on the deflection and astigmatism coil to determine to what extent miss-wounding a coil affects the corresponding magnetic field. Coils of both astigmatism and deflection that was already measured will have turns de-wound. Hopefully this will yield an understanding of what errors are possible from the coil supplier as well as the effects they could have in the machine.

## 3.3 Data Processing

To enable, ease and hasten evaluation of the measurements the data must go through processing. Processing was carried out in MATLAB by first collating the data and then extracting one full period of the trigger data. In these measurements the trigger data consists of the modulated current from the frequency generator and amplifiers run through the coils. It is measured by the current probe. The trigger signal is filtered with 50 filter samples using a rational transfer function. The filter function name is called "filter" in MATLAB. The numerator

$$B = 1 - \exp\left(-\frac{1}{filtersamples}\right) \quad (3.1)$$

and denominator

$$A = \exp\left(-\frac{1}{filtersamples}\right) \quad (3.2)$$

are the polynomials fed into the filter function. The filtering is done to reduce variance of the trigger signal easing the extraction of the trigger periods.

The extracted trigger period is used to identify the corresponding periods in the X-, Y- and Z- field data picked up by the coils on the measurement probe. The signal

picked up is a  $\frac{dv}{dt}$  that needs to be integrated which is done against the trigger signal period.

Thereafter the measured data is ready to be further processed in MATLAB to extract the required and wanted information to be analysed. One of the major challenges of this thesis is to sort through the big sets of data collected from each measurement. At every measurement point the field strength in X-, Y- and Z-axis is sampled for one period of the signal going into the amplifiers. These can all be matched according to need. For example, taking the field strength in X-axis for a combination of YZ-points in multiple X-planes of the coil to see how continuous the field strength in the focus coil varies at different lengths into the coil. Another example is to take the combined field strength and angle of the YZ-measurements in multiple X-planes to show magnitude and direction of field in an astigmatism coil.

## 3.4 MATLAB code

The MATLAB code used in the overall data processing was created by Antonio Caiafa at GE Global Research, US. It includes filtering, period extraction, integration and mapping and overall code structure. However, most parts have been modified to fit the needs of this thesis work such as the period extraction. It was not made to accommodate a signal with a DC offset as used in the focus coil. All of the 2d-plots and all code related to presentation of data has been created by the author.

# 4

## Results

In this chapter the results found will be presented. It starts with the reasons and changes made to the measurement setup to satisfy the needed repeatability of the setup. Thereafter the results of the lens measurements will be presented.

### 4.1 Measurement Repeatability

In this section problems found and their solutions with regards to repeatability is presented.

#### 4.1.1 Probe to Coil Alignment

The initial rig had severe issues with the ability to position the coil consistently. The coils were placed on top of a plastic cube with a V-shape cut-out as seen from the side. Seeing as the stepper motor stages were mounted on a separate plate to the coil mount, the alignment would never be consistent.

A 900 mm long aluminium base plate with evenly spaced screw holes was acquired on which the stepper motor assembly was mounted in one end and a coil-mount in the other as is seen in figure 4.1. The coil-mount was made up of two V-shaped optical lens holders that holds a ceramic tube. The tube used is the same sort of tube used to mount the magnetic lenses on the inside of the machine. Thus, it has a tight fit with the coils.

The LabVIEW program was also changed to help with aligning the probe to the coil. This was achieved by adding the functionality to not only set the starting position for the X-axis but also for the Y- and Z-axis. Introducing this eliminates the need for manual adjustment of the zero-position whenever the field mapper control box has been shut down, since that resets the zero-position to the default value.

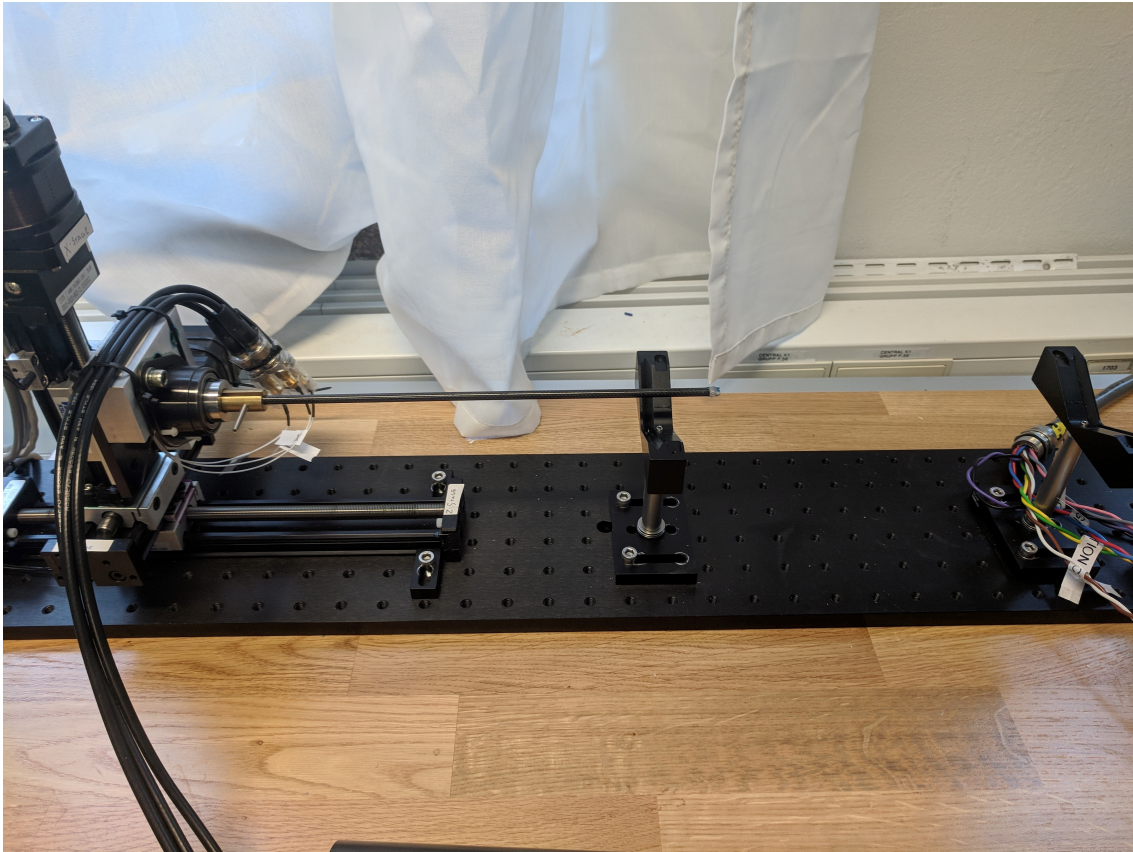


**Figure 4.1:** Added aluminium base plate with V-shaped holders and stepper motor assembly lined up. New carbon fibre probe is also visible.

### 4.1.2 Field Probe

The initial field probe had several issues that had to be addressed. Being made by glass the probe had in unfortunate accidents lost reach where parts of it had been snapped off and it was taped up. The lack of reach made it impossible to measure symmetrically outside of both sides of the coil without turning the lens around. Since it was taped the probe was not rigid anymore thus the top was moving in between measurements. Another problem was that it had only the possibility of measuring X-field and either Y- or Z-field since it only had two coils and had to be rotated. Therefore, every measurement had to be done twice in order to get the full field picture.

The solution was to manufacture a new probe. This was made of a carbon fibre tube to make it more durable. Three new coils were mounted on the new probe to allow simultaneous measurements of the X-, Y- and Z-field. The new coils had around 20% of the inductance of the old coils as they were smaller and wound fewer turns. This introduced issues with noise due to two sources. First being the lower signal level measured from the probe resulting in a significantly lower signal to noise level. Second being a higher receptivity to noise sources around. If this was because of

the lower signal level or due to an increased sensitivity of noise sources at the new coils was not investigated.

The primary noise source was found to be the stepper motors constantly producing disturbing electromagnetic fields as they were engaged to stay at the dictated position. However, the stepper assembly was neither subject to any significant outside force nor any heavy weights attached deeming this necessary. It was solved by turning off the stepper motors in the LabVIEW code before the trigger signal was sent thus eliminating the disturbance during the actual measurement. More noise reduction was achieved by altering measurement parameters as is described in section 4.1.5

### 4.1.3 Trigger Data Acquisition

The initial measurement setup was measuring the current flowing to the coils to use as trigger data. The current probe was clamped around one of the cables going to the coil from amplifier. The current probe was deemed inappropriate due to repeatability issues during measurements. The way the current probe works, to get a repeatable measurement, it would be necessary to add a clamping rig, thereby ensuring that the cables were run straight through the probe at the same distance from the ferrite in the clamp for all measurements. The reasoning is that the bends in the cable and a varying distance to the ferrite core slightly alters the current measured.

Instead of using the current probe the trigger signal could be sourced from the frequency generator, meaning that the trigger signal is the same as the input signal to the amplifiers. The effect being that the trigger data will be slightly ahead of the current through the coils. It is a trade-off for repeatability in the measurements. The same measurement only changing the positioning or reclamping the current probe as the source of the trigger signal is shown in the graphs in figure 4.2. What can be seen is the vast difference in repeatability when the trigger signal is changed to the frequency generator.

Although using the frequency generator introduces another source of uncertainty since the frequency generator is more consistent than the amplifiers. The amplifiers work by using an automatic control loop trying to keep the current driving the coils consistent. They will not be able to perfectly replicate the wave form going into the amplifier. Thus, resulting in a mismatch in the current used to drive the coils and the trigger data that is used in the data processing. Another problem using the frequency generator is that any induced dynamic effect such as resonance between coil and amplifier will go unnoticed.

A more repeatable measurement is achieved by measure the voltage over current measurement resistors close to the output of the amplifiers. Current measurement

## 4. Results

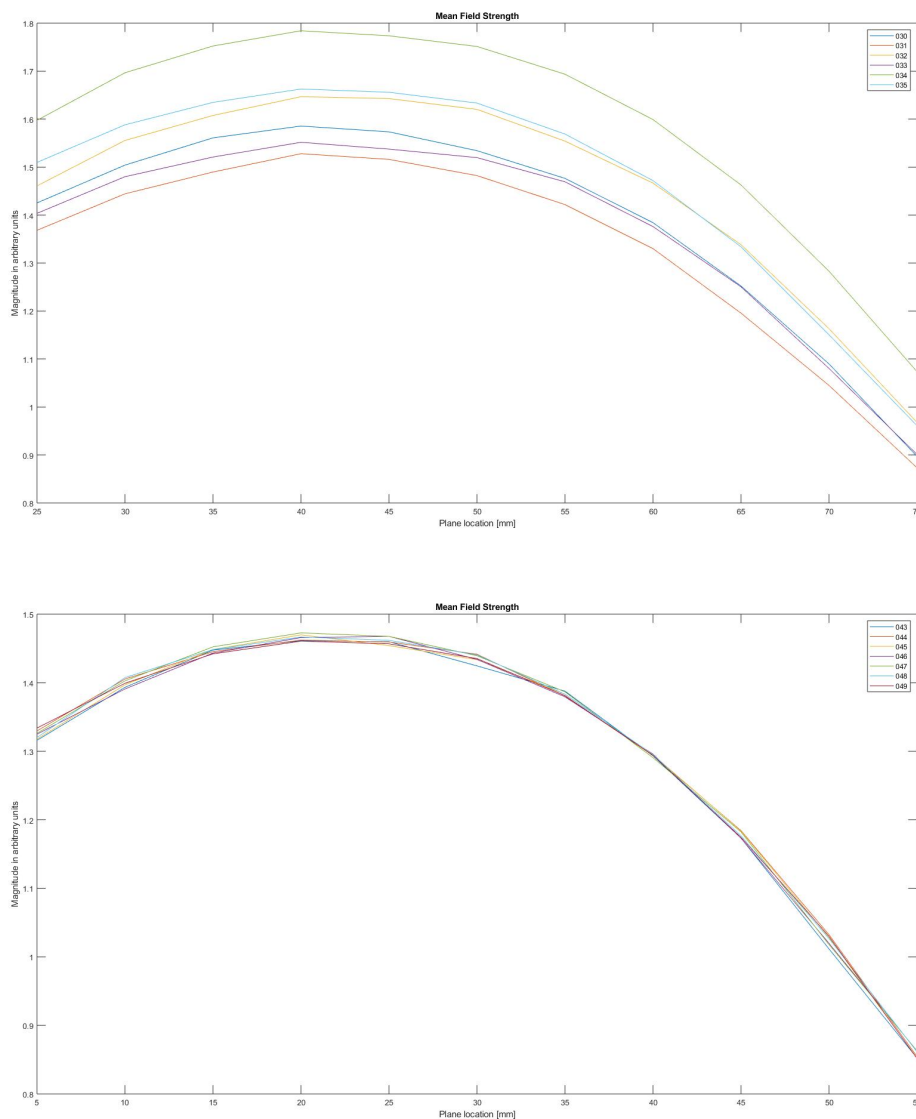


**Figure 4.2:** Focus lens measurements using the current probe as trigger signal on the top and using the frequency generator as trigger signal in the bottom. Optical axis into the coils in mm at X-axis and average plane field magnitude in arbitrary units on Y-axis.

resistors are resistors with a precise and low resistance allowing measurement of the voltage over the known resistance to accurately determine the current [10]. Measuring the current this way gets rid of all the problems introduced by using the frequency generator. A comparison of the two trigger signals can be found in figure 4.3. In this figure the inconsistency of the amplifier in recreating the signal is also demonstrated in the difference between the two peaks for the amplifier out signal. Ideally these two peaks should look the same and if they did, it would be less problematic to use the frequency generator signal as the error would be systematic. With a changing current going out of the amplifier the difference between amplifier out and frequency generator signal will be random, thus inconsistent. Another ex-

ample is demonstrated in how different the amplifier out signal looks depending on the individual amplifier. In figure 4.4 one peak for deflection X and deflection Y respectively, is shown.

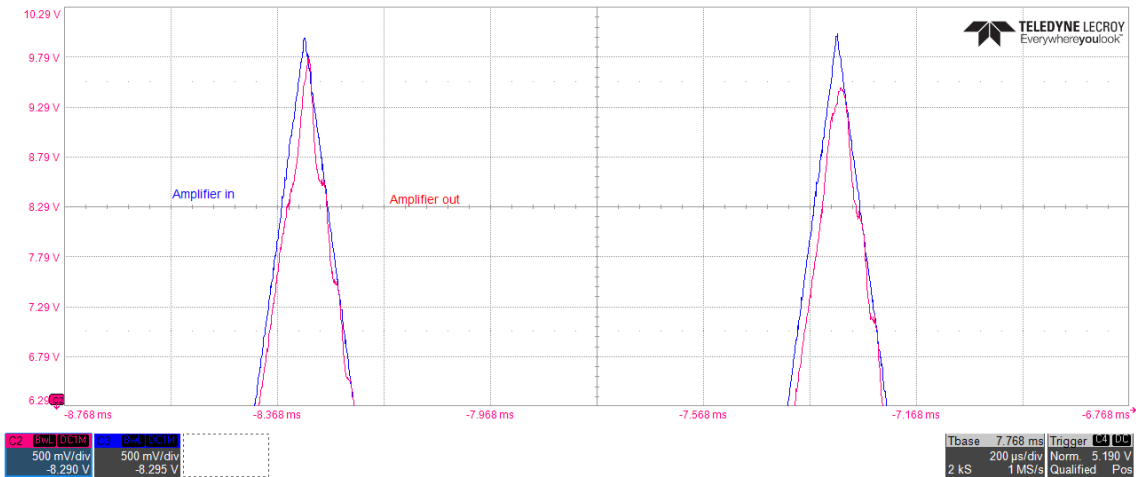


**Figure 4.3:** Difference between two different peaks from the same amplifier for the same input signal is show with red lines. The blue lines represent the signal going into the amplifier from the frequency generator. The magenta lines represent the signal out from the amplifiers into the coil.

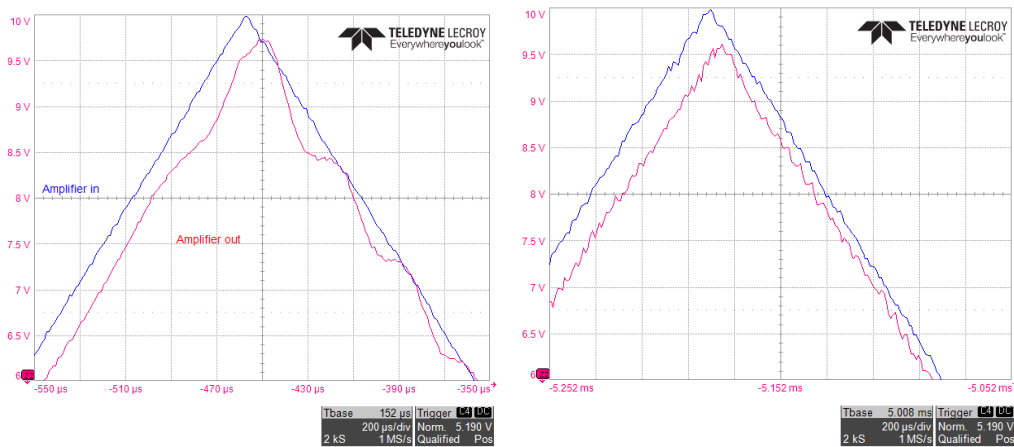


**Figure 4.4:** Difference between amplifier out for deflection X amplifier on the left against deflection Y amplifier out on right. Blue lines represents reference signal from frequency generator signal and magenta lines represent signal going out from amplifier into the coil.

A comparison of using the current feedback measurement to using the frequency generator is shown in figure 4.5. The upgrade from the frequency generator also seems to slightly reduce noise after data processing which indicates a better match as also seen in the figure.

## 4. Results

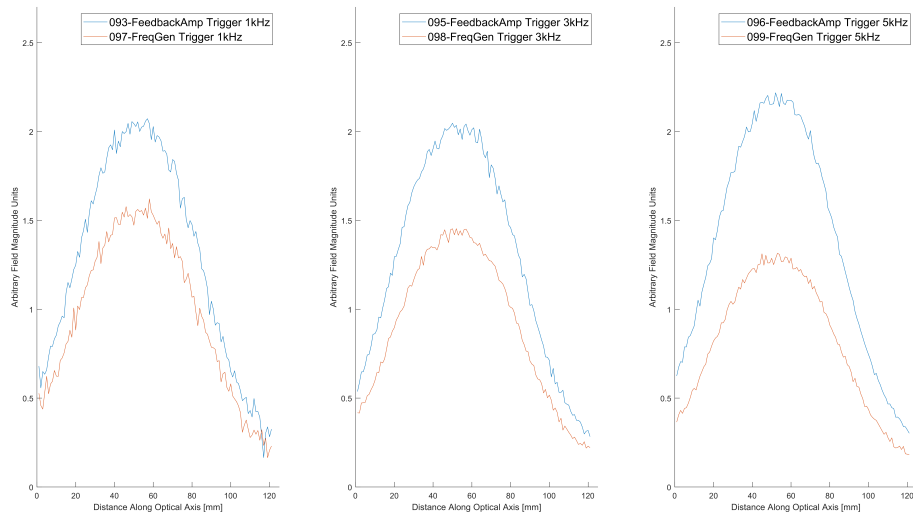


**Figure 4.5:** Comparison of using frequency generator and using the current feedback measurement from the amplifier as trigger signal over different frequencies.

### 4.1.4 Measurement Point Density

The point density is how close the measurement points are in a plane or in between planes. Depending on what quality of the lenses that is supposed to be studied different point densities are needed. Two measurement point system, as can be viewed from the LabVIEW program, is shown in figure 4.6. One has 37 points per plane and the other 255 points per plane. Translating that into astigmatism measurements is shown in figure 4.7. Depicted is two measurements of the astigmatism lens that has the two different points densities. In this measurement you can appreciate the increase in resolution by lowering the point spread.

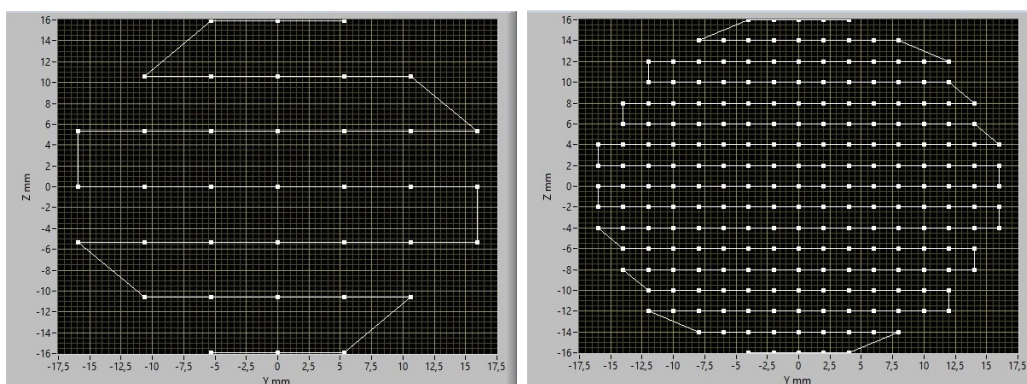


**Figure 4.6:** The different point spreads as seen in LabVIEW with 37 points on the left and 225 points on the right.

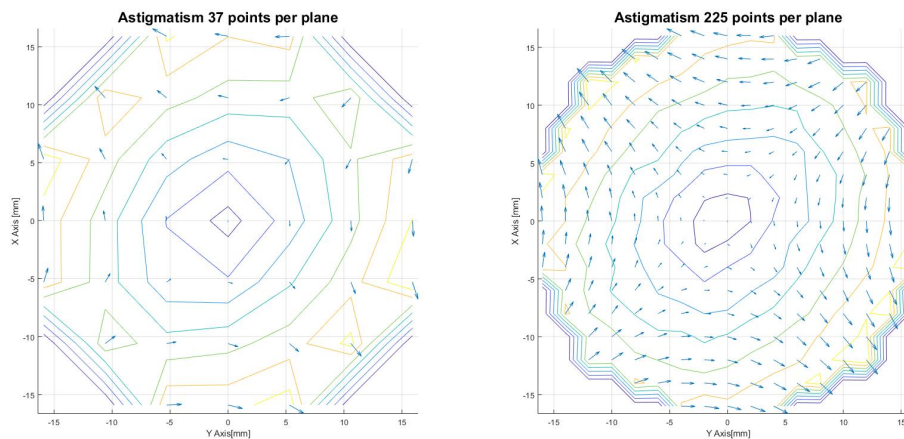


**Figure 4.7:** Showing of resolution difference using 37 points per plane in the left images versus 225 points per plane in the right for the astigmatism coil.

### 4.1.5 Instrument Parameters

In the oscilloscope and frequency generator there are possibilities to change the parameters used to affect the measurements. Namely frequency, steering signal shape, sampling rate and input impedance and their effect will be presented from the standpoint of the instruments generating them.

#### 4.1.5.1 Frequency Generator

The amplifiers and field probe is frequency dependent in this system. The amplifiers have a harder time to accurately reproduce the shape that is fed into them from the frequency generator at higher frequency. The Amplifiers used are designed for maximum frequencies of up to 20kHz. The closer you get to that limit the more the output shape is distorted. This can be seen in a comparison in figure 4.8, where the output signal from the amplifier is compared to the input signal from the Frequency generator.

Since the output from the amplifier is used as trigger signal the integrated fields measurement would not be affected that much from a distorted signal. However, the amplifiers get a harder time reproducing the same "distorted" shape over many measurements. That would introduce repeatability issues.

The field probe on the other hand is affected by the frequency in a sense that the signal and noise level is changed. A quick overview of different frequencies and magnitudes are shown in figure 4.9. The average of the X-field in each plane is

## 4. Results

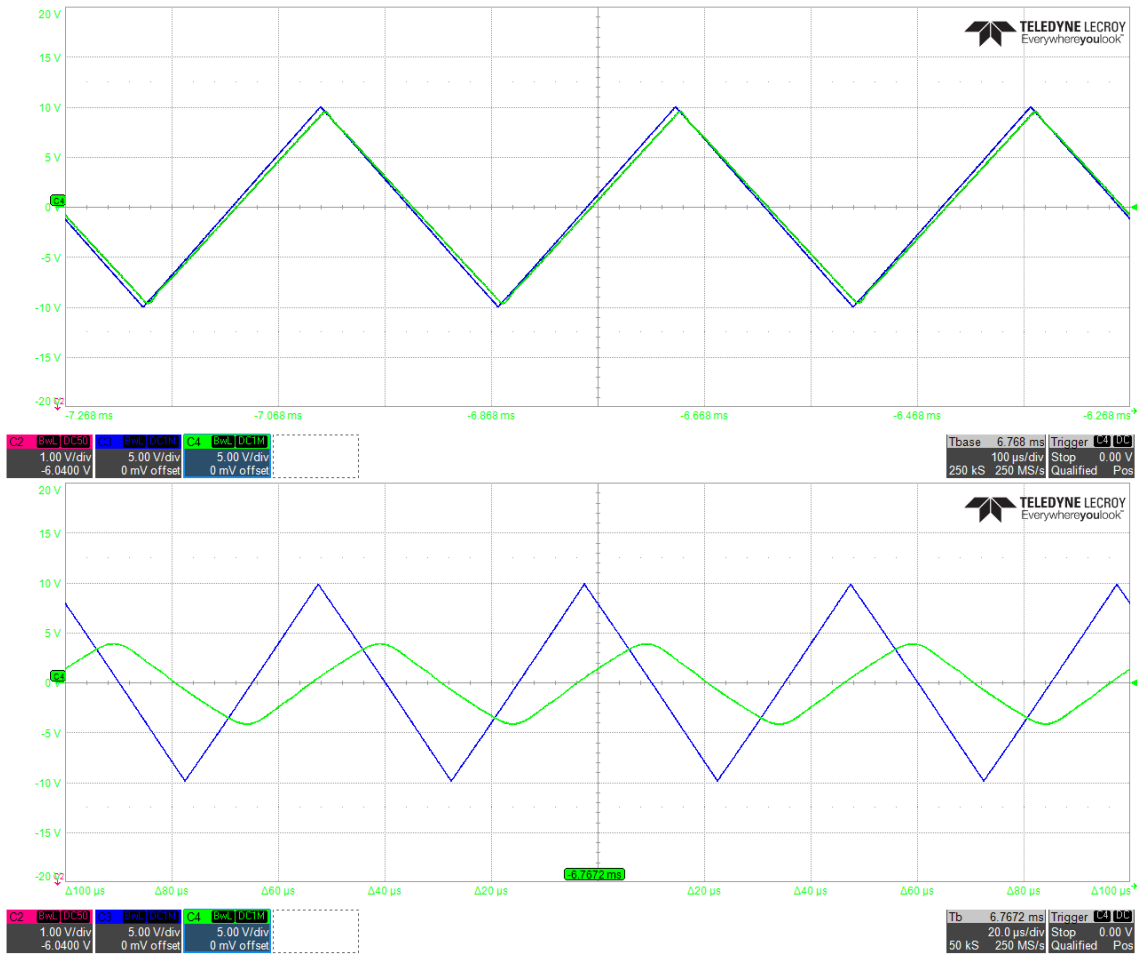


**Figure 4.8:** Frequency dependence of the output of the amplifiers (green) compared to frequency generator output at 3kHz in the top picture and 20kHz in the bottom picture

shown, magnitude of only one measurement point along the center or optical axis, difference between highest magnitude measurement and lowest measurement point and standard deviation in each plane.

### 4.1.5.2 Oscilloscope

With every measurement it is necessary to ensure that you are sampling with sufficient rate to make sure you are not missing any information. In the measurements the sampling rate is set to 1MS/s since the frequency used is only 3kHz. An indication can be found in figure 4.10 where we can see that increasing the sampling rate to 10MS/s does not change the measurement much. Seen in the different graphs are different values of the focus coil extracted from measured data used for the comparison.

The introduction of the 3-axis carbon fibre field probe introduced higher noise levels

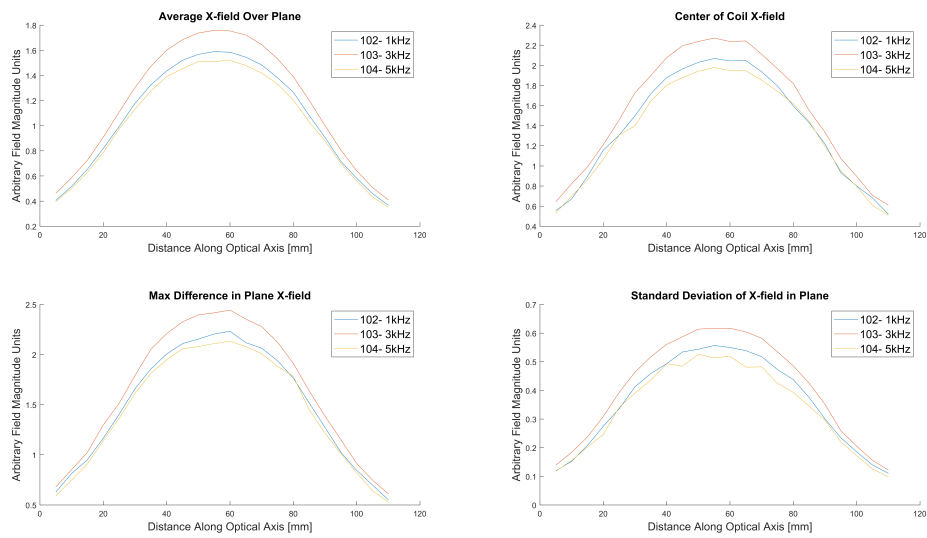


**Figure 4.9:** Magnitude in graphs is consistently frequency dependent for four different measurement criteria.

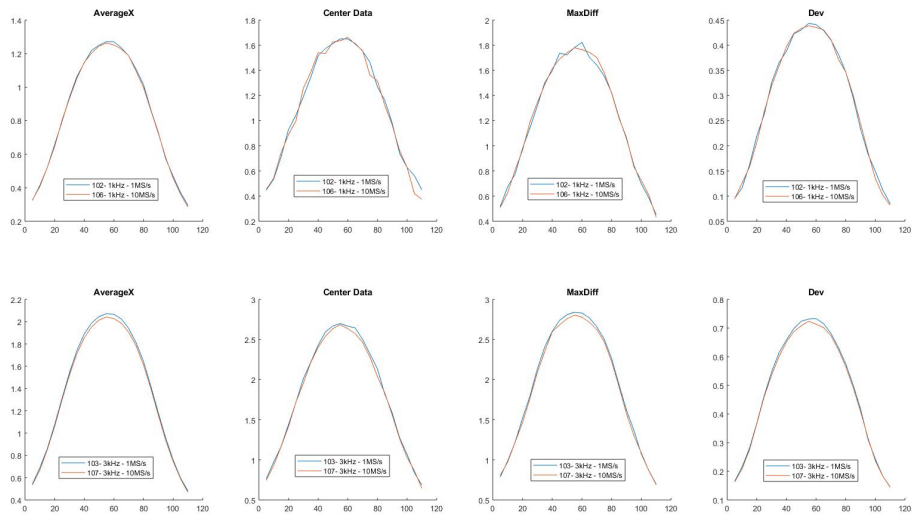


**Figure 4.10:** Figure showing magnitude consistency for plotting plane average, only centre point, max difference in plane and standard deviation over frequencies 1kHz and 3 kHz over the two sampling rates 1MS/s and 10MS/s.

as described in section 4.1.2. Noise picked up by the probe was reduced by limiting the bandwidth of the signal going into the oscilloscope. The oscilloscope used has a possibility of setting a 20MHz low pass filter which reduces noise while still preserves the signal integrity. Noise difference between 20MHz and allowing the full spectrum is shown in figure 4.11.

## 4. Results

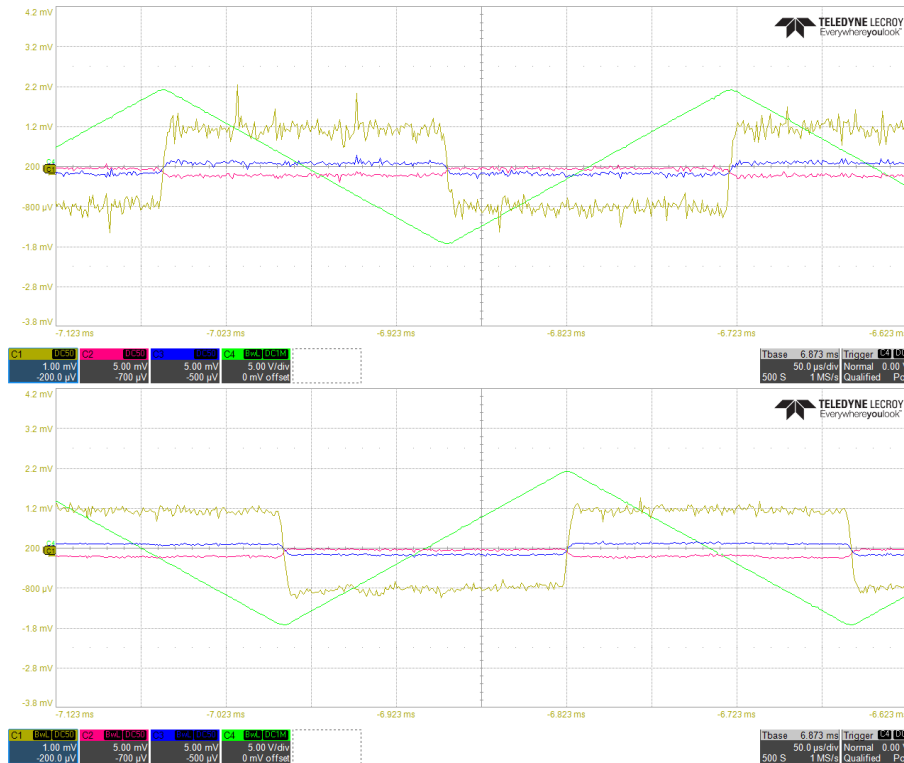


**Figure 4.11:** Difference between not using low pass filter on the field signal in the top graph compared to using 20MHz low pass filter on the field signal in the bottom graph. Especially visible looking at the yellow signal.

### 4.1.6 Final Measurement Rig

The changes to the measurement rig as a consequence of the repeatability measurements consists of; coil-probe alignment with the aluminium base plate and coil holders, carbon fibre 3-axis probe instead of glass 2-axis probe, trigger signal source replaced from current probe to current measurement of amplifier feedback signal, LabVIEW changes to enable a digitally set starting position, noise reduction by disabling stepper motors during measurement. Equipment changes has been entered into table 4.1. The final setup is also displayed in figure 4.12.

**Table 4.1:** Measurement equipment used in the final setup.

Equipment	Model	Serial no	Internal No
Oscilloscope	Lecroy HDO6034	LCRY3556N06023	EI 003
Frequency Generator	BK Precision 4052	388G17108	N/A
Focus Amplifier Rack	Arcam 103819-05	17450009	N/A
Ast/ Deflection Amplifier Rack	Arcam 103818-04	17450007	N/A
Power Supply	Peak Tech 6135	0415363004532	EI 027
Field Probe	Carbon fibre probe	N/A	N/A
Field Mapper Control Box	N/A	N/A	N/A
Stepper motors	N/A	N/A	N/A

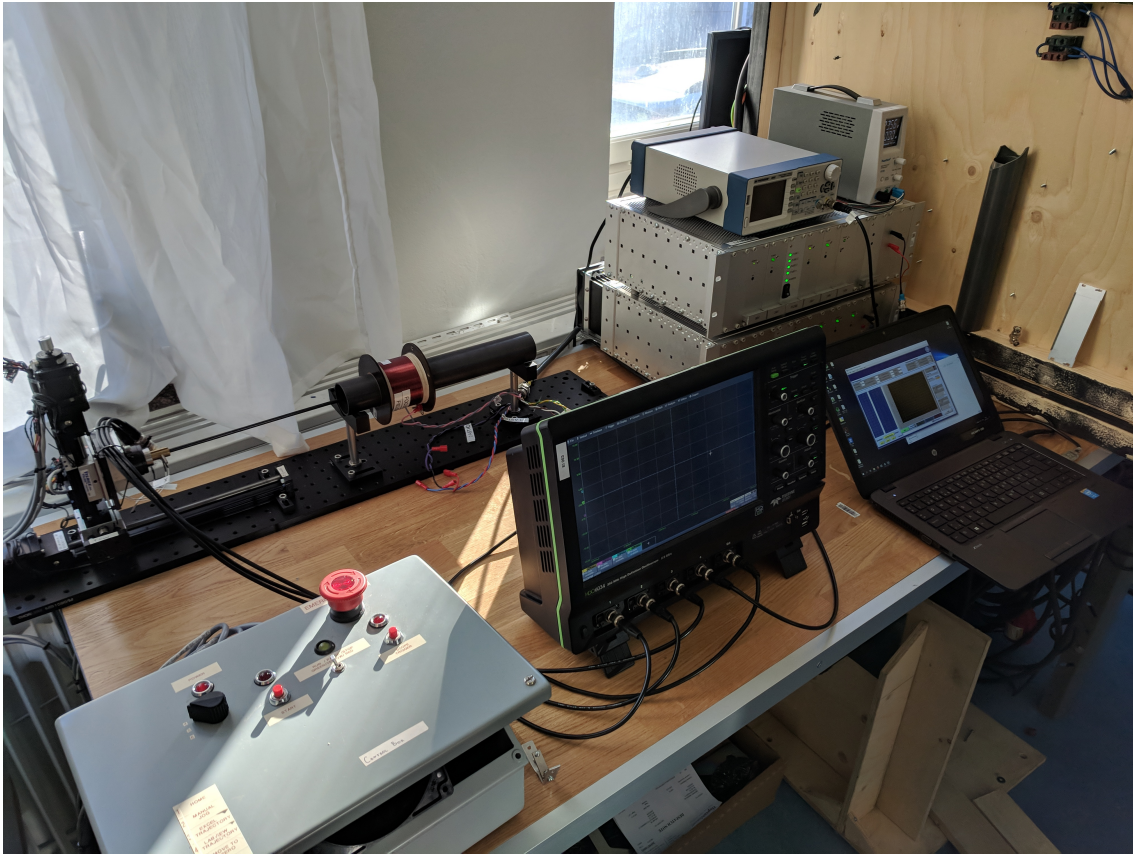


**Figure 4.12:** Depicting the setup of the final measurement rig.

## 4.2 Probe Calibration

A rough calibration of the new field probe has been done by fitting an ideal representation of a finite length solenoid to focus lens measurement data. The representation of the field at a point along the optical axis is described by rewriting Biot-Savart's law as

$$B_x = \frac{\mu_0 n I C}{2} R^2 \int_{x_1}^{x_2} \frac{dx'}{((x - x')^2 + R^2)^{3/2}} \quad (4.1)$$

where  $\mu_0$  is the permeability of free space.  $n$  is the number of turns the coil is wound per unit length,  $L$ , defined as

$$n = \frac{N}{L}$$

$I$  is the current in amperes,  $x_1$  and  $x_2$  is the start and end of the solenoid along the optical axis,  $R$  is the radial distance from the optical axis to the windings. The solenoid used in the focus coil has more than one layer meaning that the variable  $R$  will change depending on the loop. Assuming all the turns on the coil is placed at

## 4. Results

the same distance results in

$$R_{mid} = R = R_{min} + \frac{R_{max} - R_{min}}{2}$$

thus simplifying the expression. The shape of the ideal B-field lined up very well with the measured data allowing the use of only one constant,  $C$ , in the curve fitting. Curve fitting was done using a non linear least square fit in the curve fitting toolbox in MATLAB.

The focus lens measurement data is the data from the five different coils tested in section 4.3. The average of the five measurements was taken to reduce any influence from particularly noisy measurement points. The result of the curve fitting is presented in figure 4.13. The constant  $C$  acquired is 0.0163 where the inverse of  $C$ ,  $C^{-1} = 61.2745$  is the calibration constant that will be multiplied in the data processing to ensure that the measurements show at a higher accuracy to absolute values. This assumes that the model of the solenoid used is a sufficiently close representation of the actual lens. The model used gets similar values as the simulation of the focus coil presented in section 2.4.

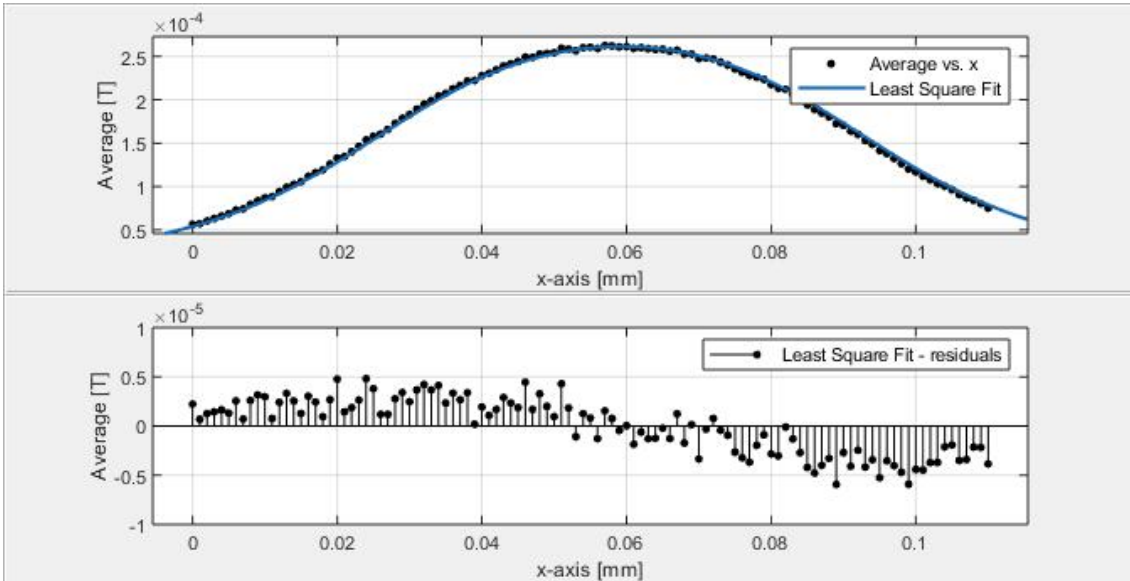


**Figure 4.13:** The least square fit line fitted to the average focus coil data is shown in the top graph and the residual of the fitting is displayed in the lower graph.

### 4.3 Average Lens Measured Data

Two of the three different lenses, focus and deflection lens, was investigated with five different lenses of each kind. The results of the measurements will be presented in the following sections along with the point densities and other parameters. The equipment in table 4.1 is what has been used. Parameters used for the measurement

can be found in table 4.2. Specific parameters will be presented for each lens.

**Table 4.2:** Parameters used in the measurements

Parameter	Value
Sampling rate	1MS/s
Frequency	3kHz
Input impedance	50 ohm
Bandwidth	20MHz
Filter Samples	50
Frequency generator signal shape	50% ramp
Field extraction level	6.3V

### 4.3.1 Focus Lens

Each focus lens was measured twice, one centre data measurement series with a higher spatial resolution along the optical axis and one lower resolution of the full interior of the lens. Centre measurement series and the full interior measurement series was done using point a spread as defined from the values shown in table 4.3. Specific parameters used for the focus lens measurement are defined in table 4.4.

**Table 4.3:** Point spread for the two focus lens measurements

Centre point measurement series	
Total points	111 points
Points per plane	1 point
Plane to plane resolution	1 mm
Full interior measurement series	
Total points	851 points
Points per plane	37 points
Point to point in plane resolution	5.3 mm
Plane to plane resolution	5 mm

**Table 4.4:** Specific focus lens parameters

Parameter	Value
Oscilloscope trigger level	6.0V
Processing trigger level	6.1V
Frequency generator DC offset	6.0V
Frequency generator amplitude	$1.0V_{peak-to-peak}$

Centre point measurement is shown in figure 4.14 in which the field along the optical axis or X-axis is presented. The differences between the measurements are not very large though the noise present is not negligible.

## 4. Results

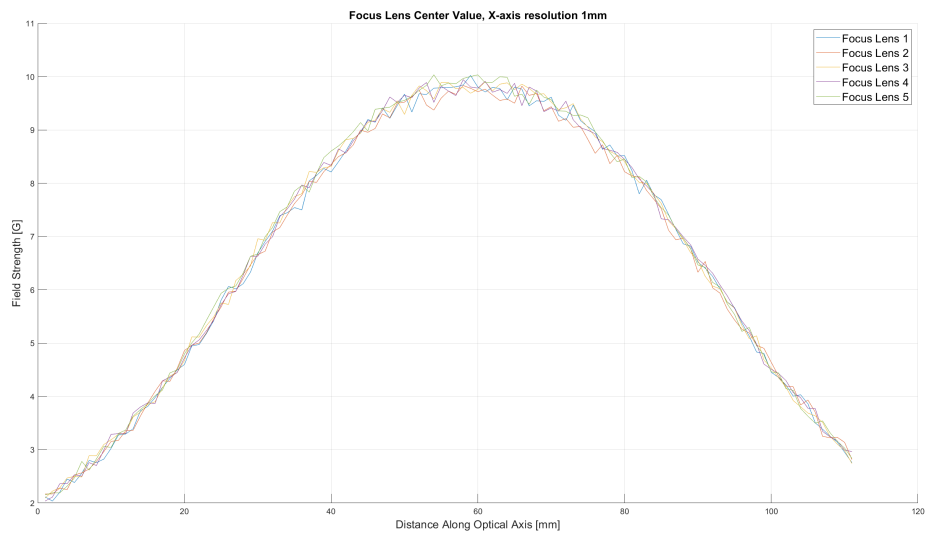


**Figure 4.14:** Centre point measurement of X-field for five different focus lenses.

The full interior measurement is split up with averages of the X-axis field in one graph and YZ-plane in one plot is presented in figure 4.15. The resulting data looks more or less the same as in figure 4.14 but smoother, less noisy.

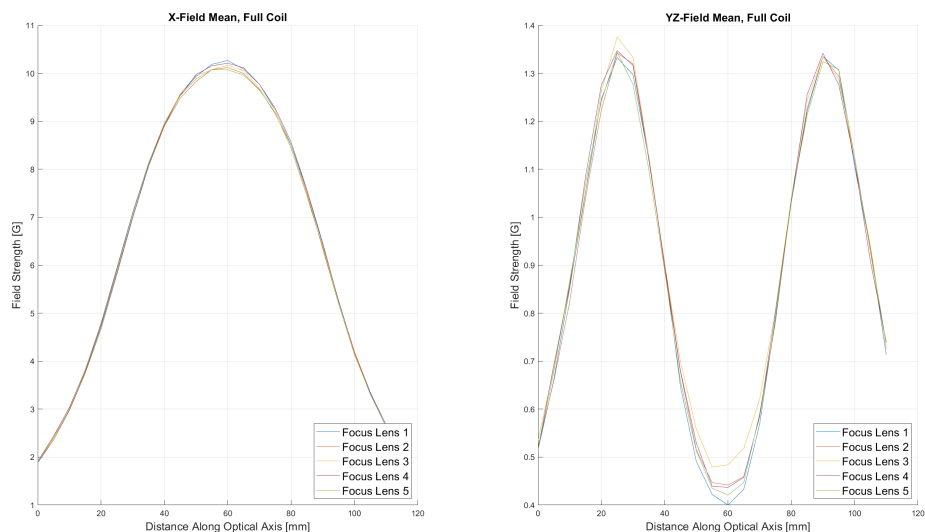


**Figure 4.15:** Full interior point spread measurement of five different focus lenses with the average of the data of X-fields in left graph and YZ-Field in the right.

The full interior measurements were also split up into an outer circle consisting of 16 points, an intermediate circle consisting of 12 points and a centre with 9 points. These different areas are presented in the graphs in figure 4.16 and figure 4.17 where X-field and YZ-field is presented respectively. Notably the difference in overall magnitude for the focus lens is pretty similar for the different areas as well,

which indicate a quite homogeneous magnetic field within the coil. The different focus lenses did not differ in any significant way to each other.

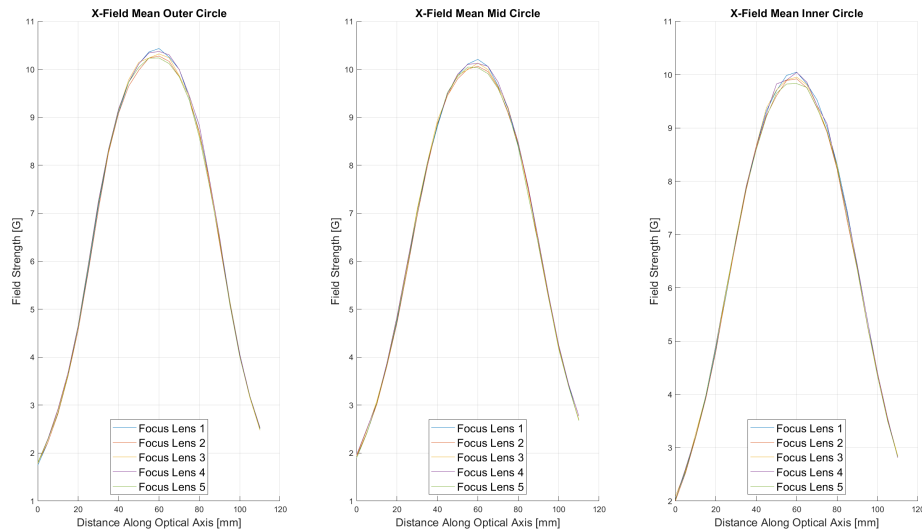


**Figure 4.16:** Full interior point spread measurement of five different focus lenses split into outer, mid and inner circle areas with respective average X-fields.

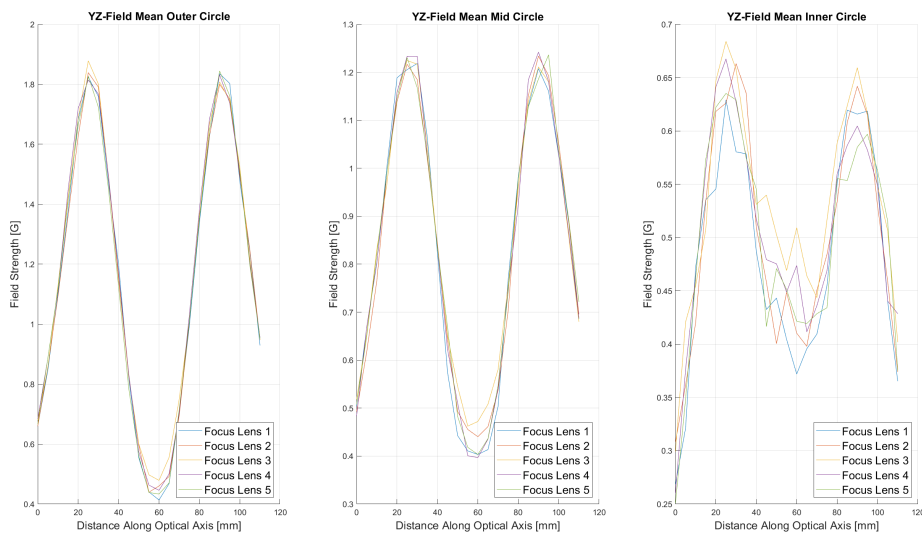


**Figure 4.17:** Full interior point spread measurement of five different focus lenses split into outer, mid and inner circle areas with respective average YZ-fields.

### 4.3.2 Deflection Lens

The deflection coil was measured using the same full interior measurement point spread as was done with the focus coil which is defined in table 4.5. The specific

## 4. Results

parameters used for the deflection coil is defined in table 4.6. Each deflection coil was measured three times, one for each dipole, deflection X and deflection Y, and one powering both dipoles at the same time.

**Table 4.5:** Point spread for the three deflection lens measurements

Full interior point spread	
Total points	851 points
Points per plane	37 points
Point to point in plane resolution	5.3 mm
Plane to plane resolution	5 mm

**Table 4.6:** Specific deflection lens parameters

Parameter	Value
Oscilloscope trigger level	0.0V
Processing trigger level	5.0V
Frequency generator amplitude	20.0V <sub>peak-to-peak</sub>

Five deflection lenses' average YZ-field is presented in figure 4.18. A wide spread in the magnitude between the lenses is shown. The lenses did not display any other significant disparities.

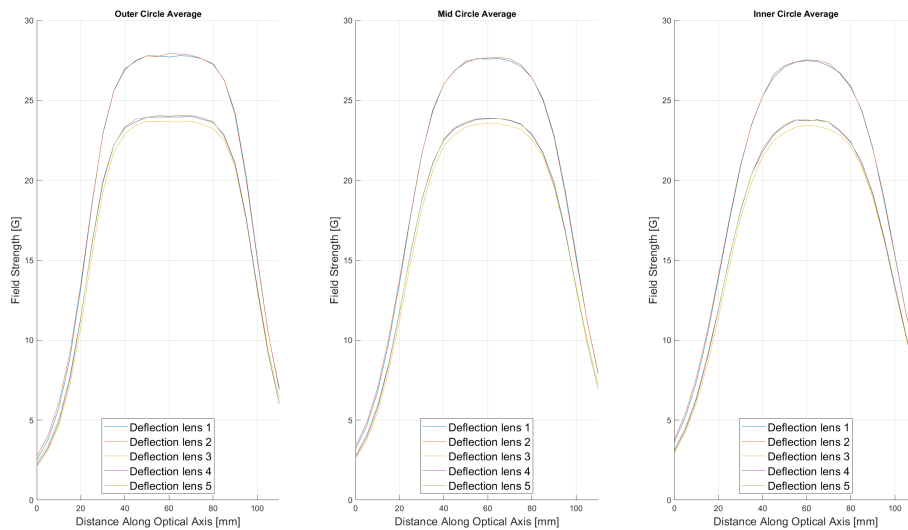


**Figure 4.18:** Full interior point spread measurement of five different deflection lenses split into outer, mid and inner circle areas with respective average YZ-fields.

## 4.4 Coil Winding Errors

The deflection lens and the astigmatism lens was measured both before and after de-winding turns on the coil to see how prone they are to winding errors during

manufacturing. The results are presented in respective section.

#### 4.4.1 Deflection Lens

The deflection lens was measured using the same settings as in section 4.3.2. Two of the already measured lenses were de-wound to varying lengths in two alterations and then remeasured. The results of the two deflection lenses is shown in figure 4.19 and figure 4.20. No significant changes were noted in these measurements.

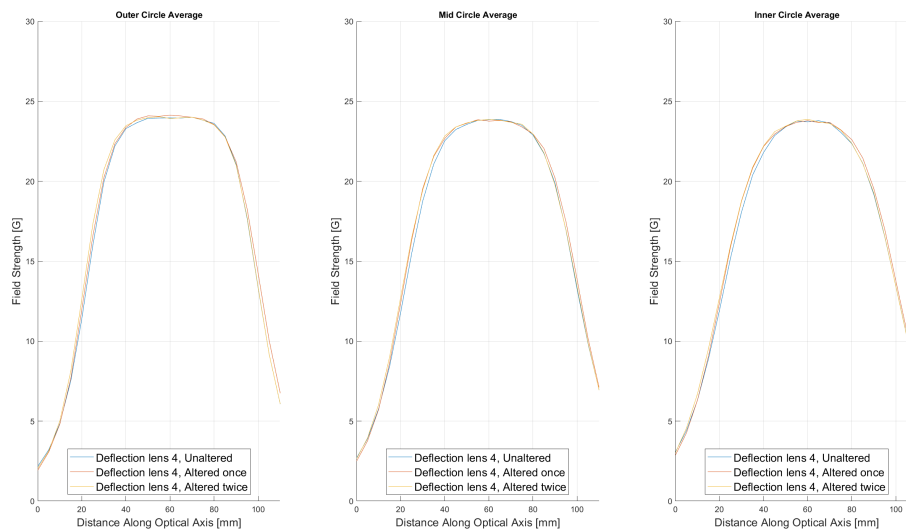


**Figure 4.19:** Full interior point spread measurement of an unaltered deflection lens and for two alterations removing varying lengths of wire from the same lens split into outer, mid and inner circle areas with respective average YZ-fields.

#### 4.4.2 Astigmatism Lens

The astigmatism coil was measured powering both quadrupoles at the same time. The full interior was measured using a higher point to point in plane resolution than both the deflection and the focus coil as is defined in table 4.7. Using the 37 points per plane, as shown in 4.7, results in a resolution yielding crude results if the zero-field area the main interest. Therefore, the coil was measured in a high resolution, using 225 points, for only three planes. The astigmatism specific parameters are listed in table 4.8.

## 4. Results

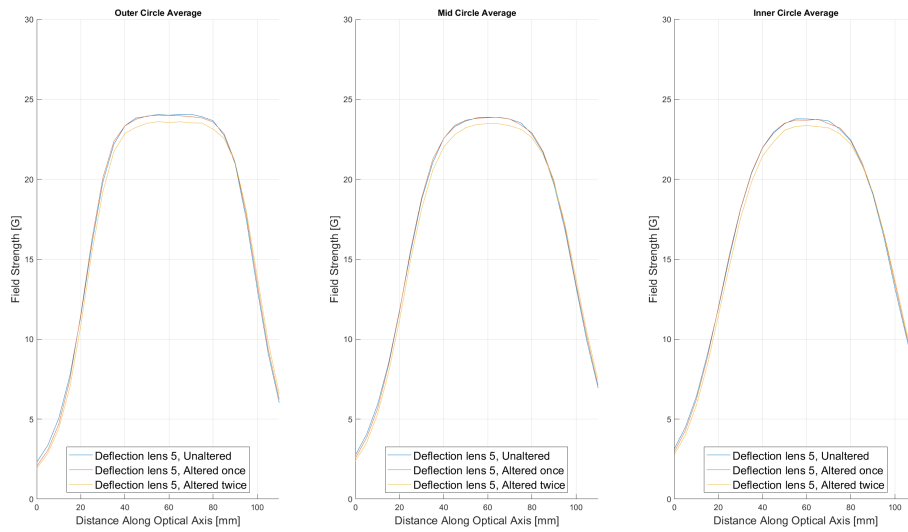


**Figure 4.20:** Full interior point spread measurement of an unaltered deflection lens and for two alterations removing varying lengths of wire from the same lens split into outer, mid and inner circle areas with respective average YZ-fields.

**Table 4.7:** Point spread for the astigmatism coil measurements

Full interior point spread	
Total points	675 points
Points per plane	225 points
Point to point in plane resolution	2 mm
Plane to plane resolution	30 mm

**Table 4.8:** Specific astigmatism coil parameters

Parameter	Value
Oscilloscope trigger level	0.0V
Processing trigger level	5.0V
Frequency generator amplitude	20.0V <sub>peak-to-peak</sub>

The astigmatism lens were, as with the deflection lens, de-wound to varying lengths in one alteration and then remeasured. The difference is depicted in figure 4.21 where the mid section of both lenses are compared and one can see that the zero-field centre changes significantly with the de-wounding.

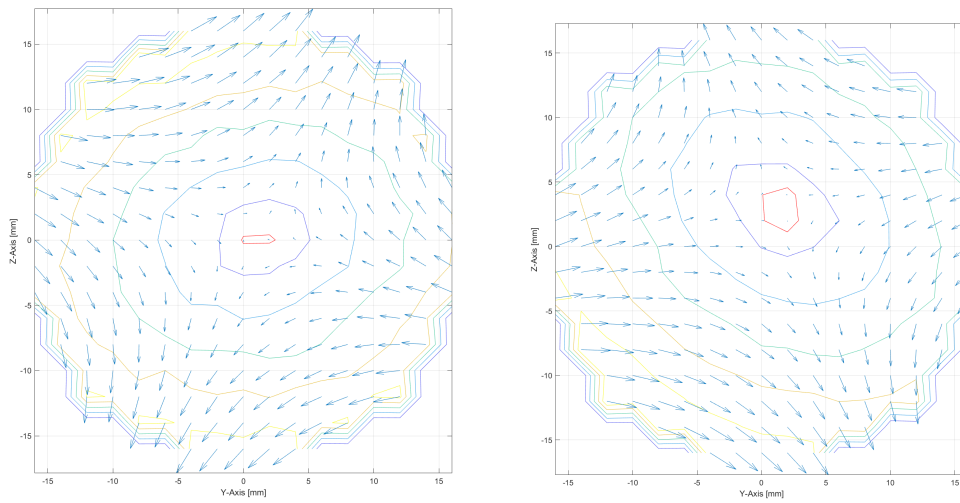


**Figure 4.21:** Mid section of the astigmatism was measured and then some turns was dewound and removed, the two measurements are compared above.



# 5

## Discussion

### 5.1 Measurement Uncertainties

Although a thorough analysis of the measurement uncertainties was not done during this thesis, the goal of the repeatability process was to reduce measurement errors to a level that would not significantly affect the interpretations. A setup capable of ascertaining high accuracy measurements is not required by Arcam at this point. The main use of the setup will be to have a separate test for the lenses, outside the machine, enabling tests on individual new prototype coils as well as effects of neighbouring lenses or external disturbances.

The following section will describe different parts of the setup where uncertainties have been found or are prone to exist. The parts described are the ones the writer has deemed most important other parts have been excluded, being considered less relevant.

Probe to coil alignment was improved drastically with the introduction of the aluminium base plate. Still the way the stepper motor assembly is mounted on the plate it can be placed at an angle to the optical axis. The differences can be measured though they are not significant enough to alter the measurement interpretation. Despite having the evenly spaced screw holes on the base plate there is still some wiggle room allowing for small angle differences from the optical axis over the whole 900mm long base plate.

The measurements rely on the fact that the small field coils in the top of the field probe are angled straight against its intended measurement axis. A small deviation from the intended angle changes the field pick up. Since the probes used, both the new carbon fibre probe and the old broken glass probe, are handmade these unorthogonalities exist, introducing systematic errors into the system.

Another difference between the new and old probe is that the new probe is built of smaller coils wound with fewer turns thus reducing the size of the probe. Unfortunately this reduces the sensitivity of the coils raising the lowest field magnitude

possible to measure. A positive side effect is that the coil is smaller allowing for measurement of the fields with higher spatial resolution, which is beneficial in the case of the astigmatism lens. The higher spatial resolution also applies to what is considered to be the centre point of the measurement. The bigger pick-up coils used the larger the distance from the centre of the coil to the centre point of the measurement. This effect is amplified by having multiple coils in the probes.

### 5.2 Trigger Data Acquisition

The most important change in the measurement setup was done to the way the trigger signal was sourced. Using the current probe as trigger signal turned out to be detrimental to the repeatability of the field mapper. Using the frequency generator output as the trigger signal was deemed very repeatable. However, it introduced both uncertainties about resonance between coil and amplifier as well as a time shift in trigger signal compared to the picked up field signal.

### 5.3 Average Correct Coils

Noise in the focus lens centre measurement depicted in figure 4.14 can also be due to of the tolerance factor introduced in making sure a sample is found for the requested current in the data processing. It is not certain there is a sample at the wanted current. Thus, a non-insignificant change in current is introduced in the extraction of the fields between the field planes. The code used for the extraction could be optimised for a smaller tolerance. This does not account for all the noise however which leaves the noise picked up by the field probe as well as the noise affecting the trigger signal from the amplifiers. Both of which could be improved to receive less noise, by making a more field-sensitive field probe and shield the trigger signal cable inside the amplifier as well as outside as is done now.

The focus lenses, if the noise can be disregarded, looks very similar to each other implying the manufacturing is sufficiently robust. The measurements can also be used as a vague confirmation that the field mapper works as intended. No significant differences are found in the measurements as is expected from such a simple solenoid lens.

The deflection lenses showed a bigger variation in the YZ-field than was expected. The variation is quite significant showing differences of over 10% between comparable lenses. However, this is not EBM-process significant since the process calibrates away the difference, by running a higher magnitude lens with slightly less current.

## 5.4 Coil Windings Errors

All of the coils used in finding winding errors have problems with rotation and alignment along optical axis since they are not glued anymore. This complicates comparisons of rotational dependent values such as investigations of change in the deflection lenses field rotation. The lenses were also affected by the dismantling process introducing uncertainties for the results achieved while investigating the winding errors.

For future studies the rotation of the de-wound lenses could have been better kept track of. The inner coils of the lenses after dismantling rotates freely and in the current setup it is hard to get them consistently in the same rotation. Making sure the rotation is the same can give more insight into the field change and would be subject to future studies of the magnetic lenses.

No significant changes was seen from changes made to the deflection lens and what was found could either be related to dismantling effects or is insignificant when compared to the variance of the unaltered lenses. A tendency to desymmetrise the lens was detected, it was however too vague to draw any clear conclusion. Therefore, the author cannot draw any conclusions about changes to the deflection lenses after de-winding the coils hence warranting further studies to investigate winding errors of the deflection lens.

An interesting revelation was instead found during measurement of the de-wound astigmatism lens. It appears that the centre of zero-field of the lens is significantly altered by removing turns from the coil. Further investigation of astigmatism field quality should be commenced to see how this drastic change in zero-field centre is affecting the prevention of higher order astigmatism that the lens is used for. More thorough measurement series of more lenses should be undertaken to understand the changes that can occur and also ensure that no improperly wound lenses are supplied to Arcam.

## 5.5 Future Work

Future work involving the field mapper can be split into two categories. First there are improvements to the actual setup that can be done. These would be primarily pursued if more accurate measurements are needed. Secondly would be future use of the field mapper for measurements and further analysis of measurement data.

Improvements to the setup should be pursued depending on future intent. To add another, more sensitive, probe would allow for measurement of fields further away from actual coil or for new lenses wound fewer turns or run with a smaller current.

However, before doing that a characterisation of the current probe would be a good start to determine the sensitivity.

To make the measurements with smaller errors a better and more well made probe with regards to the alignment of the pick-up coils would be needed. The probe needs to be calibrated through a validated process as well. Complementing the new probe an overview of the alignment on the base plate should be done, both for the stepper motor assembly as the zero-position within the coil.

A more thorough study of frequency dependence of the system would also be welcome to see if there are possibilities extending sensitivity or get less noisy measurements.

Future measurements that the field mapper could be used for would for example be an investigation in various effects of a combination of the lenses. This would be done to look at interference, dynamic and synergy effects between lenses. At the same time an interesting question to answer is how long the settling time for the field is for the different lenses and their combinations.

External field effects on the magnetic fields inside the lenses is another interesting thing to study. To build upon the review of the settling time from lens combinations a natural increment is to look at the effect external fields has on the settling time of the fields. Another increment could be to look at the transient field and other dynamic effects with external interference from possibly one of the vacuum pumps.

An extensive review of the data that was measured during the process of writing this report should be undertaken. The measurement method amasses a substantial amount of data that can be processed and examined to a much greater extent than what has been done. The many ways the data can be interpreted and presented can yield new knowledge or deeper understanding.

# 6

## Conclusion

The thesis outlines the process and describes the major obstacles overcome in achieving a setup sensitive and robust enough to validate and measure the magnetic coils used in Arcam's EBM technology. A host of small changes with corresponding measurements have been done to pinpoint and isolate their effect on the measurements. The most notable change was made to the field mapper in changing the trigger signal resulting in a drastically improved repeatability. Changing the field probe was necessary to carry out the measurements intended however, it introduced an increased susceptibility to noise that had to be reduced to manageable levels. This was done through an investigation of the different changeable parameters and code in the system such as powering down the stepper motors, frequency, input impedance and trigger signal.

A characterisation of the magnetic lenses has begun. The focus lens has been mapped and no significant errors or differences were found in the meagre sample of five lenses investigated. Although a small sample, the defects in focus lens is deemed to be of low risk due to the ease in manufacturing of the simple geometry. Deflection or astigmatism lens however with higher manufacturing complexity should be considered more carefully. The deflection lens was mapped and although showing a wide spread in magnitude the effect of the differences is considered to be handled in the EBM-process thus having low impact.

Removing turns of the deflection lens seemed to show signs of changing the symmetry in the lens. Otherwise no significant changes were detected with the data processing and handling that was used. Therefore a more precise investigation should be undertaken if the effect of removing turns is enticing. Making sure the rotation of the coil is highly consistent as well as using a less noise sensitive probe is used would be advised to increase the improve the measurements.

The most notable result was found in measurements of the astigmatism lens, where removing turns of the coil significantly altered the position of the zero-field centre. A more thorough study of the effects of improperly wound lenses should be undertaken. An investigation of what new aberrations are introduced and how the de-wounding affects the zero-field position and the lens' ability to counteract higher order astigmatism should be part of this study.



# Bibliography

- [1] R. Huang et al. "Energy and emissions saving potential of additive manufacturing: the case of lightweight aircraft components," *Journal of Cleaner Production*, vol. 135, pp. 1559-1570, Nov, 2016. <https://doi.org/10.1016/j.jclepro.2015.04.109>, [Online]- Available: ScienceDirect.com, <https://www.sciencedirect.com/science/article/pii/S0959652615004849>, Accessed on: 2018-08-30.
- [2] S. Ford, M. Despeisse, "Additive manufacturing and sustainability: an exploratory study of the advantages and challenges," *Journal of Cleaner Production*, vol. 137, pp. 1573-1587. Nov, 2016. doi:<https://doi.org/10.1016/j.jclepro.2016.04.150>, [Online]. Available: ScienceDirect,<http://www.sciencedirect.com/science/article/pii/S0959652616304395>, Accessed on: 2018-10-01.
- [3] M. J. Donachie, "Ingot Metallurgy and Mill Products," in *Titanium : A Technical Guide*, 2nd ed. Materials Park, OH : ASM International, c2000, ch. 4, pp. 25-32. [Online]. Available: ProQuest Ebook Central <https://ebookcentral.proquest.com/lib/chalmers/detail.action?docID=3002373>. Accessed on: 2018-10-01.
- [4] Arcam EBM Brochure, Mölndal, Sweden: Arcam EBM, n.d. [Online]. Available: <http://www.arcam.com/wp-content/uploads/arcamebm-corp-brochure-fnlv3.pdf>, Accessed on: Sept 21, 2018.
- [5] P.W. Hawkes and E. Kasper. *Principles of Electron Optics*. Ed. by P.W. Hawkes and E. Kasper. Vol. 1. San Diego: Academic Press, 1996, pp. 3–14. isbn: 978-0-12-333340-7. doi: 10.1016/B978-012333340-7/50180-0.
- [6] Ernst Ruska. "The development of the electron microscope and of electron microscopy". In: *Rev. Mod. Phys.* 59 (3 July 1987), pp. 627–638. doi: 10.1103/RevModPhys.59.627.
- [7] David K. Cheng, "Static Magnetic Fields," in *Field and Wave Electromagnetics*, 2nd ed. Reading, Mass., USA: Addison-Wesley Pub. Co, cop. 1989, pp 225-306.
- [8] R. F. Egerton. *Physical Principles of Electron Microscopy: An Introduction to TEM, SEM, and AEM*. 2nd 2016. Cham: Springer International Publishing, 2016. isbn: 9783319398778.

- [9] P. Grivet, "CHAPTER 10 - STRONG FOCUSING LENSES," in *Electron Optics* (Second Edition), P. Grivet, n.d: Pergamon, 1972, ch. 10, pp. 287-322.
- [10] D. W. Braudaway, "Precision Resistors: A Review of the Techniques of Measurement, Advantages, Disadvantages, and Results," *IEEE Transactions on Instrumentation & Measurement*, vol. 48 no. 5, pp. 884-888, Oct 1999. doi: 10.1109/19.799640, [Online]. Available: IEEE Explore Digital Library, <https://ieeexplore.ieee.org>, Accessed on: 2018-10-01
- [11] Frisk, D. (2016) A Chalmers University of Technology Master's thesis template for  $\LaTeX$ . Unpublished.